STATIC LIQUEFACTION OF LOOSE GRANULAR LANDSLIDES

by

Liam James Steers

A thesis submitted to the Department of Civil Engineering

In conformity with the requirements for

the degree of Master of Applied Science

Queen's University

Kingston, Ontario, Canada

(October, 2018)

Abstract

Highly mobile landslides can have devastating impacts on infrastructure and human life. In order to mitigate the risks of these landslides, it is critical to understand how they are triggered and the mechanism behind their high mobility. The objective of this research is to investigate the initiation and propagation of liquefaction and the resultant flow mobility due to static triggering in loose granular slopes using two physical modelling techniques. The first experiment used geotechnical centrifuge techniques to determine the velocity of the liquefaction propagation in saturated granular slopes for loose and dense soils, by varying the thickness and void ratios of the materials. The results of these tests indicate that all model slopes which were loose of the critical state were highly liquefiable upon shearing, while all dense tests resisted liquefaction and instead were subject to erosion as they could withstand much higher seepage flow rates. Tests that experienced liquefaction reveal that the velocity of the liquefaction propagation is not dependent on the velocity of shearing of the initial failure (0.25-0.5 m/s), and that the speed of propagation of the liquefaction front can happen at an order of magnitude faster than that of the initial triggering event (4.2-4.3 m/s). A second series of experiments was performed to develop testing techniques and best practices for dam breach experiments using a large-scale flume. In this test series, both saturated fine sand and coarse grained material were examined. Results from testing the saturated coarse grained material show that landslide mobility increases with respect to dry flow when the material is saturated. As expected, the increase in mobility with the addition of water is due to the proportional decrease in basal shear resistance. In contrast, the same experiment with fine sand did not experience failure and most of the material remained in the release box. This surprising finding indicates the possible significant role of air entry and matric suction on the higher strength in the latter case and indicates an interesting avenue for future research to quantify this phenomena.

Acknowledgements

Queen's Staff

Thank you for all the assistance you have given me over the last few years. Willie and Graeme, thanks for all the support out on West, but more importantly, thanks for the barbeques!

C-CORE

Thank you to Dr. Rodney McAffee, Dr. Ryan Phillips, Gerry Piercey and Karl Kuehnemund. Thank you for all your help during the late nights and jam-packed days of testing.

Ellis 101

Thanks for the memories. It was a great 2+ years. Thank you for your help in the lab during my many, many attempts to get my experiments to work. My back thanks you.

Dr. Baller

Crazy to think we started our undergraduate degrees together and now we're finishing our respective graduate degrees together at "roughly" the same time. Thanks for being a great friend, but more importantly, thanks for letting me do laundry at your place when I made the horrible decision to live above a nightclub. Lesson learned.

Family

Thank you for always believing in me and encouraging me every step of the way. I'm sure we all learned a few really cool things about landslides during this time!

Hayley

To my loving wife, Hayley. Thank you for everything you have done and continue to do. Most importantly, thank you for making sure I still ate vegetables during this final push.

Andy and Ryley

I cannot begin to thank you enough for all the patient guidance and tireless support you have given me over the course of this adventure. From hours of debugging code together, to troubleshooting technical issues from halfway across the country, to ceaseless edits, I couldn't have done this without you.

Table of Contents

List of Figures

List of Tables

List of Abbreviations and Symbols

α	Fahrböschung angle
α_g	Travel angle
DAN	Depth averaged numerical method
dN’	Effective normal stress
DIC	Digital image correlation
FEM	Finite element method
Hz	Hertz
LE	Limit Equilibrium
N	Centrifugal acceleration
PPT	Pore pressure transducer
PWP	Pore water pressure
Q	Ground water flux
r_u	Pore water pressure ratio
u	Pore water pressure
σ_v	Total vertical stress
τ_B	Basal shear resistance
φ	Friction angle

Chapter 1

Introduction

1.1 General

In practice, analyses of triggering and mobility of liquefiable granular slopes are typically performed separately and treated as two separate stages. Triggering analyses are primarily performed using a limit equilibrium (LE) method. These analyses are typically based on the most unfavourable, yet credible, pore water pressure expected at the site of interest. When using the method of slices to determine slope stability, LE analyses involve the solving of equilibrium equations of the interslice forces. Various methods of LE slope stability exist with methods satisfying the equilibrium of horizontal forces, moment forces or both. One of the more common methods is the Morgenstern-Price method developed by Morgenstern and Price (1965), which is applied while conducting analyzes using numerical modeling software.

The numerical modeling software that is widely used for slope stability analysis is the Slope/W program developed by GEOSLOPE. Figure 1.1 gives a representation of a free body diagram of the interslice forces that govern slope stability. The symbol dN' denotes the effective normal force for the respective slice. With the introduction of pore water pressure, a decrease in the effective stress occurs, thereby reducing the resisting force and bringing the slope closer to the triggering point of failure. While LE methods are exceedingly useful to assess slope stability, these methods provide no information with regard to how mobile the landslide debris will be as well nor the extent of their potential zone of impact. In order to predict landslide mobility, dynamic shallow flow modeling is often used to determine the zone of impact of the landslide, such as the work performed by Hungr (1995). DAN-W, a program developed by Hungr, is often used by geoscientists and engineers to predict landslide runout and determine the severity of the hazard. This software is based on the assumptions of the landslide consisting of a shallow flow and having a thickness at minimum an order of magnitude less than the entire length of the flowing

mass. Physical properties of the modeled landslide, including the basal rheology, are user-defined (Hungr & McDougall, 2009). If the basal rheology is assumed to be frictional, then an introduction of pore water pressure (PWP) will increase the mobility of the landslide. Water reduces the basal shear resistance, proportionally increasing the landslide mobility.

As stated earlier in this section, landslides are often analyzed using either a triggering or mobility approach, however, for landslides that experience liquefaction these two approaches are inherently coupled. The initial shearing failure can induce excess pore water pressure which proportionally decreases shear resistance and increases mobility. This is exemplified in the case study of the La Conchita, California landslide in 2005. In 1995, the slope mobilized causing minor property damage. The slope then remobilized in 2005 after a period of intense rainfall and simultaneously and nearly instantly transitioned into a highly mobile debris flow resulting in ten fatalities and destruction of property (Jibson, 2006).

1.2 Landslide Mobility

Highly mobile landslides, such as La Conchita, pose a significant risk to those living in mountainous areas or at the base of large hills. These flows are highly unpredictable and difficult to control. Slopes that have been deemed as safe and stable can suddenly mobilize and do considerable damage. Significant effort has been invested in determining the parameters that control the potential for these highly mobile flows to occur. In order for a slope to be liquefiable, the soil must be sufficiently loose such that the void ratio is greater than the critical state void ratio at the given stress state. The critical state parameter, which was determined via triaxial testing, is the state at which unlimited turbulent deformation occurs while normal stress, shear stress, and void ratio remain constant (Roscoe et al., 1958). Granular material with a void ratio higher than the critical state will experience liquefaction under rapid loading and shearing if the conditions are undrained. If the void ratio of the sample being tested is lower than the critical state void ratio at the same confining stress, then the soil will be dilative and liquefaction will not occur. This emphasizes the fact the void ratio plays an important role in the control of soil stability.

Past work in numerical modeling has attempted to quantify the difference in runout potential given a small incremental change in void ratio from the critical state. Iverson et al. (2015) performed numerical modeling of the Oso, Washington landslide. This site is of specific interest due to the site's history of landslide activity as noted by the identification of ancient headscarps from air photos, such as in Figure 1.2. In 2006, this slope mobilized and dammed the nearby river, however the mobility of the failed slope was minimal in comparison to the event that occurred in 2014. The 2014 event mobilized at the same location, however this event had a distal reach far greater than the preceding event and was the cause of several fatalities. Figure 1.3 depicts the outcome of the 2014 event. In the Iverson study, the porosity of the soil was changed between consecutive models and the results showed that at a void ratio change of only 0.02 greater than the critical state was the difference between a highly mobile liquefaction event and a small slumping dilative failure. The results of the numerical modeling performed by Iverson (2015) and reproduced herein as Figure 1.4, display the difference between a dilative slump and highly mobile liquefaction event. These results also add validity to the theory that void ratio plays a large role in landslide mobility. However, as often is the case with the back analyses of field case studies, details on the pre-failure soil properties are unknown, analyses must be conducted by assuming soil parameters.

In addition to numerical modeling, physical modeling has also been conducted to examine the mechanisms governing slope liquefaction. Take and Beddoe (2014) performed geotechnical centrifuge models using a fine sand to investigate slope liquefaction under static loading. This research program observed that liquefaction occurs preferentially at the toe of the slope along the base. At this location, the soil is easily saturated with a looming triggering mechanism in waiting to shear the soil.

In the case of the 2014 Oso slide, as described by Keaton et al. (2014) and Iverson et al. (2015), it is known that the event occurred from a remobilized slope, much like it did in the La Conchita case. The initial slump failure quickly sheared the saturated base which resulted in the slide rapidly transitioning to a highly mobile flow. The research from Take and Beddoe (2014) and Iverson et al. (2015) show the exact two stages that occurred in Oso: the base is required to shear for liquefaction, and then, when the

soil is sufficiently loose, it can become highly mobile. However, there is the unknown element of just how rapidly the liquefaction of the base occurs. It is apparent when modeling landslides that the model must be conducted as a complete analysis, rather than in separate stages. Analyzing the landslide as a whole will provide insight into the degree of mobility of the flowing mass and the type of mechanisms that control the velocity of liquefaction propagation.

1.3 Research Objectives

This research program was designed to investigate the mobility of saturated loose granular material upon shearing. This was achieved using physical modeling techniques with a geotechnical centrifuge and a large-scale landslide flume. Specifically, the objectives of this research program were to:

- Investigate the speed and propagation of the liquefaction front using high-speed camera footage to record the evolution of landslide velocity and volume, and a dense sensor network of PWP sensors to quantify the distribution of excess pore water pressure. This can be used to determine whether or not the velocity of the liquefaction front can exceed the velocity of the initial event.
- Investigate the shear behavior of saturated granular material within dam break experiments and develop testing techniques and best practices.

1.3.1 Physical Modelling Techniques

The first research objective was met using a geotechnical centrifuge. The centrifuge allows for the development of prototype scale strains and stresses to be generated in a reduced-scale model. Due to the scaling of the model, testing in a centrifuge has the benefit of collecting prototype scale results in a drastically shorter timeframe. Discussion of the various scaling laws and principles has been thoroughly outlined in the literature (e.g. Schofield, 1980; Take et al., 2004; Garnier et al., 2007; Askarinejad et al., 2014). All centrifuge tests were conducted at the Centre for Cold Ocean Resource Engineering (C-CORE) located in St. John’s, Newfoundland.

The second research objective was achieved using a large-scale landslide flume and soil release box. Flume tests have the benefit of repeatedly testing large volumes of a repeatable size in a controlled environment. This research objective will enable tests to be completed to compare how the mobility of saturated granular material differs from dry flows of the same volume and boundary constraints. All flume tests were conducted at the Coastal Engineering Laboratory located at Queen's University.

1.4 Organization of Thesis

This thesis is presented in manuscript format as outlined by the School of Graduate Studies at Queen's University. Chapter 1 gives a general introduction to the topic as well as the overarching research objectives. Chapter 2 and 3 are drafts of original manuscripts and are followed by Chapter 4 which contains the overall conclusions of the research program.

Chapter 2 presents the results of geotechnical centrifuge modeling of static liquefaction triggering in granular soil and the resultant slide mobility. The results from this experimental program show that the velocity of the liquefaction front is not dependent on the velocity of the initial failure.

Chapter 3 presents the results of a research program where testing techniques have been developed for dam breach experiments. This chapter provides insight into challenges encountered, the preliminary results of saturated landslide mobility testing, and recommendations for future testing.

Overall conclusions of the dissertation are summarized in Chapter 4.

1.5 References

Askarinejad, A., Beck, A., & Springman, S. M. (2014). Scaling law of static liquefaction mechanism in geocentrifuge and corresponding hydromechanical characterization of an unsaturated silty sand having a viscous pore fluid. *Canadian Geotechnical Journal*, 708-720.

Garnier, J., Gaudin, C., Springman, S. M., Culligan, P. J., Goodings, D., Konig, D., et al. (2007). Catalogue of scaling laws and similitude questions in geotechnical centrifuge modelling. *Internatioal Journal of Physical Modelling in Geotechnics*, 3: 01-23.

Hungr, O. (1995). A model for the runout analysis of rapid flow slides, debris flows, and avalanches. *Canadian Geotechnical Journal*, 32(4): 610-623.

Hungr, O., & McDougall, S. (2009). Two numerical models for landslide dynamic analysis. *Computers & Geosciences*, 35(5): 978-992.

Iverson, R. M., George, D. L., Allstadt, K., Reid, M. E., Collins, B. D., Vallance, J. W., et al. (2015). Landslide mobility and hazards: implications fo the 2014 Oso disaster. *Earth and Planetary Science Letters, 412*, 197-208.

Jibson, R. W. (2006). The 2005 La Conchita, California, landslide. *Landslides*, 3: 73-78.

Keaton, J. R., Wartman, J., Anderson, S., Benoit, J., deLaChapelle, J., Gilbert, R., et al. (2014). *The 22 March 2014 Oso Landslide, Snohomish County, Washington.* National Science Foundation.

Morgenstern, N. R., & Price, V. E. (1965). The analysis of the stability of general slip surfaces. *Geotechnique*, 15(1): 79-93.

Roscoe, K. H., Schofield, A. N., & Worth, C. P. (1958). On the yielding of soil. *Geotechnique*, 8(1): 22-53.

Schofield, A. N. (1980). Cambridge geotechnical centrifuge operations. *Geotechnique*, 30(3): 227-268.

Take, W. A., & Beddoe, R. A. (2014). Base Liquefaction: a mechanism for shear-induced failure of loose granular slopes. *Canadian Geotechnical Journal*, 51(5): 496-507.

Take, W. A., Bolton, M. D., Wong, P. C., & Yeung, F. J. (2004). Evaluation of landslide triggering mechanisms in model fill slopes. *Landslides*, 173-184.

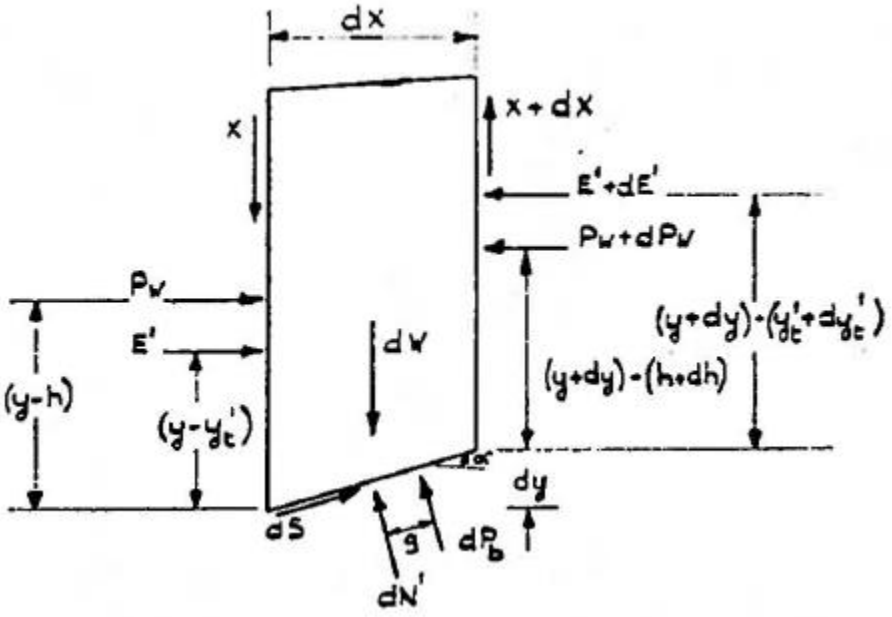

Figure 1.1 Free body diagram of interslice-forces involved in a LE analysis (Morgenstern & Price, 1965).

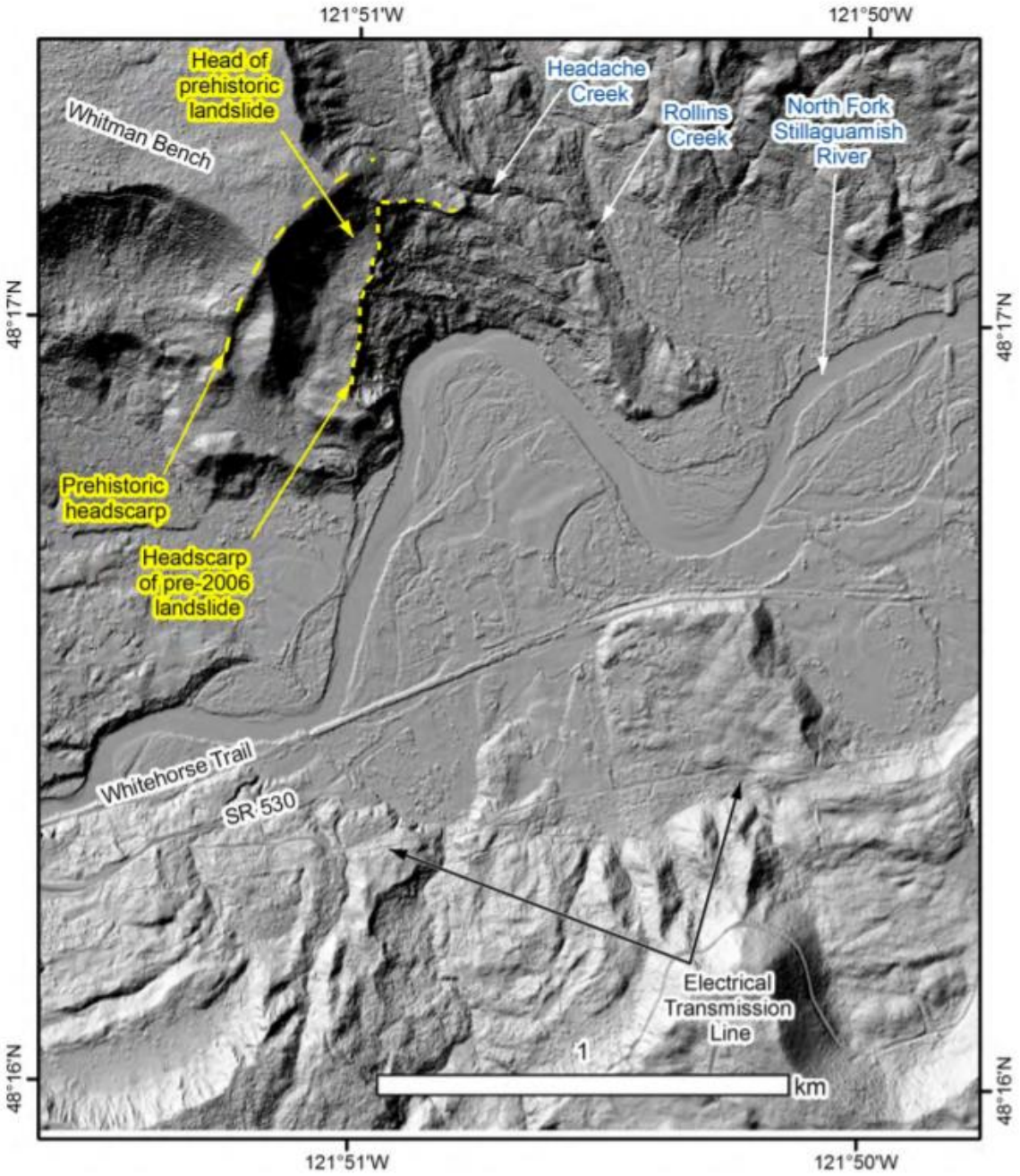

Figure 1.2 Air photo depicting the headscarp of the 2006 event at Oso (Keaton, et al., 2014)

Figure 1.3 Outcome of the 2014 Oso event (Keaton, et al., 2014)

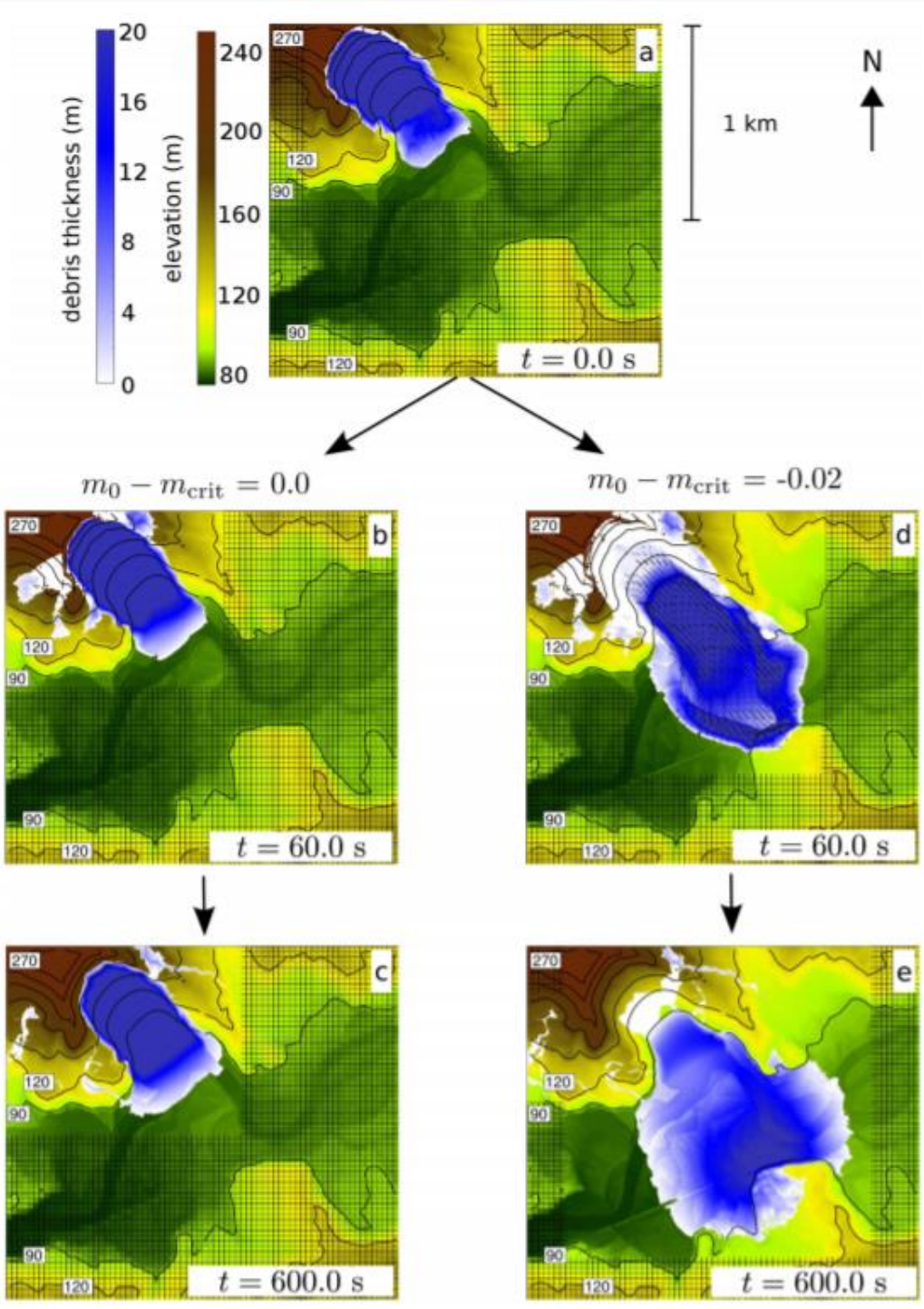

Figure 1.4 Results of Iverson, et al., (2015) numerical modeling of the 2014 Oso landslide.

Chapter 2

Static liquefaction propagation observed in centrifuge landslide models

2.1 Introduction

On March 22, 2014 the residents of Oso, Washington were struck by a landslide now referred to as the Oso Landslide (Keaton, et al., 2014). This slide was initiated on a gently sloping hill of less than 20° (Iverson, et al., 2015) and had a distal reach of one kilometer across the valley floor burying the local community of Steelhead Haven. The slide covered the local highway for 600 m and buried it with 6 m of debris. This was one of the worst cases of landslide disasters in the history of the United States with a total of 43 fatalities and an estimated $50B (USD) in economic losses (Keaton, et al., 2014). Field evidence from the site support the belief that liquefaction occurred (Keaton, et al., 2014); however, it is still unclear what mechanism triggered the liquefaction and what the exact order of events was that lead to this disaster. It has been hypothesized that an initial slope failure can trigger the liquefaction of the base of a slope. For this to happen, the base would have to be sufficiently saturated and the soil loose enough that it could be contractile and liquefiable (e.g. Take et al., 2015; Take & Beddoe, 2015). To date, the exact sequence of events that caused the Oso disaster is still unclear (Keaton, et al., 2014; Iverson, et al., 2015).

One reason why it is hard to agree on how static liquefaction events occurred is due to the lack of eyewitness evidence and data from local monitoring stations. Without a description of how the slide moved it is difficult to postulate with any degree of certainty how the event took place (Keaton, et al., 2014). Another reason it is difficult is that the rheologies and groundwater conditions at the site prior to failure are often unknown. If the soil is sufficiently loose and saturated, then static liquefaction can occur, otherwise, however if the soil is dense, then there is the possibility of a dilative failure occurring with no liquefaction (Ng, 2008). Figure 2.1 illustrates a generic scenario of how a simple rotational failure on a slope might evolve. (It should be noted that the generic scenario is not necessarily representative of the

events that occurred at Oso). In this hypothetical scenario, a small initial toe failure (Figure 2.1a) can be imagined to result in two drastically different consequences depending on the density of the soil at the base of the slope. If the base soil is dilatant (Figure 2.1b), the small toe failure induces shear stresses within this soil, resulting in negative excess PWPs and the distal reach of the landslide is small. However, if the base soil is sufficiently loose to be contractile on shearing, a significantly different outcome is possible. Such a scenario has recently been investigated in physical models by Take and Beddoe (2014) who illustrated that a small rotational failure near the toe of the slope could trigger liquefaction in the soil at the base of the landslide if it was sufficiently loose and saturated. If such a scenario were to occur as illustrated in Figure 2.1c, the shearing and entrainment of the soil at the base of the landslide could greatly increase the area at the base of the slope influenced by the landslide event.

Although it has been shown that loose contractile soil along the base of the slope will liquefy, the mechanism through which the initial landslide causes the rapid volume expansion and entrainment of the liquefied soil along the base of the slope is unknown. In particular, it is unclear whether the velocity of the liquefaction front is limited by the maximum velocity of the initial toe failure, or whether in certain circumstances it could even exceed this velocity.

The objective of this chapter is to investigate the speed and propagation of the liquefaction front in a simplified physical model using a geotechnical centrifuge. High-speed camera footage is used to record the evolution of landslide displacement, velocity, and volume, coupled with a dense network of PWP sensors is used to quantify the spatial and temporal distribution of excess PWPs. These results will enable a comparison between the velocity of the liquefaction front within the soil at the base of the landslide to the velocity of shearing observed in the base soil. The results will also allow for the velocity of the initial toe failure to be used to determine whether the velocity of the liquefaction propagation can exceed the velocity of the initial toe failure triggering the liquefaction event.

2.2 Experimental Setup and Methods

2.2.1 Experimental Program

Physical models of landslides have been used in the past to better understand the mechanisms that contribute to mass wasting events and the resultant mobility of a failed slope (e.g. Take et al., 2004; Ng, 2008; Askarinejad et al., 2014; Take & Beddoe, 2014). For this paper, a geotechnical centrifuge was used to conduct physical modeling of a saturated fine sand slope. The centrifuge allows for quick testing of smaller, more manageable physical models that correspond to larger scale models due to the scaling effects of an amplified g-level. In order to scale models from large scale to centrifuge model scale, the length, width and height of the model are scaled by 1/N, where N is the g-level of testing (Rezzoug et al., 2004). Similarily, the test duration to complete each is also scaled by the same amount.

The objectives of this study were achieved through the testing of six physical models which consisted of specimens that were either very loose and contractile or dense and dilative as characterized earlier in Figure 2.1. These six physical models differed in thickness and void ratio however, the loose tests had similar void ratios as did the dense tests. During failure of a dense soil, the soil dilates on shearing. The increase in the pore spaces between the particles does not generate excess PWP and therefore no liquefaction takes place. The opposite is true for loose soils where the soil is contractile. Under undrained conditions there is a generation of excess PWP, which leads to a runaway liquefaction event. These two separate scenarios are depicted in Figure 2.1.

2.2.2 Instrumentation

PWPs generated in the models were monitored throughout the duration of the tests using two types of sensors. Seven (7) GE-Druck PDCR-81 sensors were installed flush with the soil-bedrock contact along the base and the slope. In addition to the Druck sensors, twenty-three (23) Motorola MPX5050GP sensors were installed along the entirety of the slope and the base. The Motorola sensors were spaced at 30 mm intervals between sensors. The dense configuration of the sensors allowed for characterization of the dynamic pore pressure response along the entirety of the model. All sensors were seated along the base of

the slope and saturated before each test was conducted. This was done in order to acquire accurate PWP readings while attempting to minimize the impact the sensor opening had on the change in boundary conditions. Prior to testing and after saturation of the sensors, a thin metal filter was placed over each sensor opening. This filter acted as a porous barrier allowing uninhibited flow of the water in the model to the sensor while simultaneously inhibiting any of the soil from clogging the sensor. Sony RX10M2 was used to record high-speed videos of each test. Videos were recorded at 960 frames per second with a resolution of 1920x1080 pixels. Videos of each test were taken through the transparent sidewall at gravitational increments of 1 g, 10 g, 15 g, and 20 g and at the time of slope failure. The camera was positioned as to capture the largest field of view possible (494 x 300 mm) in order to see the maximum amount of the model (camera field of view shown in Figure 2.2). The video files recorded during the tests were used to quantify the displacement and velocity of the landslide through the use of digital image correlation (DIC). Using DIC, which compares the deformation of a defined grouping of pixels from image to image, one can perform a slope movement analysis for an area of interest within the model being tested. The DIC analysis tool used for analysis in this paper is the GeoPIV program developed by White et al. (2003). In this program, a defined set of pixel patches is used to quantify deformations. In order to track a mesh of DIC patches, some of the sand was dyed black and sprinkled along the front of the viewing window to provide contrast colour contrast during analysis. Dyeing the sand created a gradation of soil colour which the GeoPIV software recognizes as a change in pixel intensity. The change in pixel intensity allows the program to distinguish between different patches. Patch movements were measured every 1/960 s during the failure for each test.

2.2.3 Model Configuration

All six of the physical models were tested using the C-CORE beam centrifuge in St. John's, Newfoundland, Canada. The test configuration was chosen to model a thin soil layer overlaying an impermeable bedrock layer, similar to the geometry of Take and Beddoe (2014). The base was constructed from two aluminum plates. These plates had a slight taper along the width of the plates to

encourage slope failure near the viewing window. The drop across the plates was 3mm with the width of the plates being 300mm, the length of the base plate 374 mm, and the sloping plate length 481 mm. The interface friction between the soil and the aluminum plate was increased by applying waterproof anti-slip paper. Moldable sealing putty, Duxseal, was used to make the model watertight and ensure there was a no-flow boundary between the viewing window and the aluminum plates. The model setup included a sloping section angled at 30^{o} and a horizontal base as shown in Figure 2.2. A soil layer with an initial thickness of approximately 50mm was deposited along the entirety of the model. When tested at 20 g, the model would correspond to a soil thickness of 1.0 m at prototype scale assuming no consolidation of the soil on spin-up. Due to the sharp change in inclination between the sloping section of the model and the base, a low hydraulic gradient was created. A low hydraulic gradient creates a buildup of a groundwater table within the soil which is a necessary condition for static liquefaction.

2.2.4 Soil Layer

The soil used in all six tests was #730 Silica Sand by Weldon Company. This soil was used by Beddoe and Take (2016) for a large scale landslide test for which it demonstrated that it has physical properties very similar to those of the Ottawa F110 Silica Sand, which had been used in similar liquefaction studies (e.g. Take & Beddoe, 2015). Prior to the construction of each model the sand was dried to remove any residual water. After drying, water was added to a known mass of soil to achieve the desired initial gravimetric water content. This initial water content was added to the sand to encourage the development of matric suction in order create a suitably contractile soil. Soil was then rained through an ASTM No.5 sieve with 4 mm openings. Soil rain height and initial water content varied depending on the desired initial void ratio for the test. After deposition of the soil, a vacuum was used to smooth the surface of the soil to ensure an even surface. Initial void ratios ranged from 0.7 - 1.79 which is well above the sand's dry maximum void ratio. Upon spin-up of the centrifuge the models consolidated, resulting in void ratios ranging from 0.66 - 1.04.

2.2.5 Antecedent Groundwater Conditions

The groundwater in the model was introduced through a variable metered pump. By changing the voltage of the metered pump the rate of ground water flux (Q_{in}) could be controlled. For denser models, the metered pump did not have sufficient flow and an additional steady state pump had to be used in tandem. Water from the pumps flowed through a perforated pipe and a weir at the top of the slope. The weir was machined so that water would be distributed evenly along the width of the soil in the model and accounted for the curved acceleration field of the centrifuge. The water that made its way through the soil and drained out the toe (Q_{out}) was drained to the centrifuge chamber (Figure 2.2). Groundwater flow through the model was increased incrementally resulting in an increase in the groundwater table. During each corresponding increment, the flow rates were increased once steady state conditions had been achieved. Steady state conditions were determined based upon stabilization of pore pressure readings of pressure sensors imbedded along the base of the model at the sand-bedrock interface. Flow through the model was continued until a landslide occurred or erosion of the base was identified.

2.3 Testing Results

2.3.1 Testing Summary

Six tests of various thicknesses and void ratios of either condition were conducted. The first test, immediately prior to failure, had a void ratio of 0.73 and is referred to as Loose 1. The four remaining loose tests are known as Loose 2, Loose 3 and Loose 4 while the remaining two dense tests are labeled Dense 1 and Dense 2. A summary of the tests conducted can be found in Table 2.1, along with information on the model thickness as well as the test outcome.

Table 2.1 Testing summary

Test number	Initial void ratio	Thickness at 1g (mm)	Thickness at 20g (mm)	Flow Rate at Failure (mL/min)	Model Outcome
Loose 1	1.45	52.6	37.3	382.4	Liquefaction
Loose 2	1.62	56.7	37.7	259.4	Liquefaction
Loose 3	1.17	50.3	49.7	416.3	Liquefaction
Loose 4	1.79	58.8	36	222.7	Liquefaction
Dense 1	0.7	49.9	49.9	450.2	Erosion of toe
Dense 2	0.79	49.9	49.9	517.9	Erosion of toe

2.3.2 Behaviour Observed in Loose Tests

The behavior observed in a typical loose slope, Test Loose 1 (L1), is presented in this section. Test L1 had a base layer soil thickness of 37.3 mm (measured at 20 g). A stepwise increase in seepage flux within the model is shown in Figure 2.3a, where PWP data is captured by the pore pressure transducers (PPTs) and plotted as a total head at model scale above the x-location of each PPT. PPT response due to the flowing water can be seen along the base of the model, while PPTs along the slope remain mostly unresponsive as there is little build-up of water along the slope. Figure 2.3a shows that as the flux through the system is gradually increased, so too is the height of the groundwater table. The increase in groundwater table height is due to the low hydraulic gradient of the model. Similar behavior was seen in the experiments performed by Take and Beddoe (2014). Increasing groundwater is an important aspect of the testing as the soil needs to be sufficiently saturated in order to lose the additional strength provided by the intergranular matrix suction. When this suction is lost, there is a collapse of the soil that leads to a small failure and a subsequent generation of excess PWP.

The failure event in Test L1 was triggered at the toe of the slope, and the excess PWP generated as a result of the failure event are illustrated in Figure 2.3b and c. What can be seen is a clear rise in PWPs along the base of the model. However, it is interesting to note how the propagation of PWPs occurs. At first, as shown in Figure 2.3b, it can be seen that only the toe area where the initial failure occurred experienced a change in PWPs while the rest of the base remained unaffected. As the base of the model

was progressively sheared there was a spike in PWP experienced by the PPTs further away from the toe. As the soil further along the base began to experience the generation of excess PWP, the PWPs closer to the toe were already starting to dissipate (Figure 2.3c). This shows that there is a propagation or 'wave like' behavior of PWP generation across the base of the model, initiated by nothing more than a small initial rotational failure.

Liquefaction of the base can best be represented in terms of the pore water pressure ratio r_u, which is defined as the ratio of the PWP to the total vertical stress at a location. The equation for pore water pressure ratio is shown in Equation 2.1 where u is the PWP (kPa) and σ_v is the total vertical stress (kPa).

$$r_u = \frac{u}{\sigma_v} \qquad \text{Eq (2.1)}$$

As r_u approaches 1, effective confining stress approaches zero. Given these conditions, shear resisting forces drop significantly such that large accelerations can occur due to the unbalanced forces. For all tests, r_u values were calculated along the base at the location of the PPTs. PPTs along the slope were omitted as saturation levels of the soil were not sufficiently high to produce liquefaction. Figure 2.4 shows the r_u values that were calculated for test L1. A comparison was made between the r_u values immediately prior to the failure event and the maximum r_u values recorded during the failure. From Figure 2.4 it can be seen that r_u values prior to failure are ~0.5. During the event itself, r_u values approached 1 with many exceeding a value of 0.8 showing how the small initial failure caused the initiation of the shearing of the base which led to the generation of excess PWP. The large r_u values (0.8 to 1) signify that the base did liquefy, and that the liquefaction extended along the majority of the base.

The initial failure event and progressive shearing of the model that resulted were captured using high-speed digital imagery. The digital images were analyzed using GeoPIV developed by White et al. (2003). Through analysis of the images resultant displacements and velocities can be quantified to describe the slope and base movement at various time steps. Figure 2.5 shows the evolution of the slope failure with superimposed images of DIC results. DIC results are of the total displacement experienced over 0.02s intervals, capturing the movement of the model at different periods of time throughout the failure. For test

L1, it can be seen that an initial small shearing of the soil occurs in first (Figure 2.5a). This small failure transitions into a larger deep seated failure (Figure 2.5b). The failure then propagates farther along the base of the slope showing the transient nature of the event (Figure 2.5c-d). What is evident from these results is that the slope does not fail as a single mass. It can be seen that the distal end of the base of the slope is still mobile well after the initial failure event at the toe of the slope has stopped moving. The results from test L1 have shown that an initial failure event triggered liquefaction along the base of the slope, however it remains unclear how the initial failure event itself influenced the resulting speed and distal reach of the liquefied base.

For the four tests that experienced liquefaction (Loose 1-4), a DIC analysis was performed on the initial failure region (S1 shown in Figure 2.6a) to quantify the displacement and velocity of the initial failure event. Figure 2.6a I-IV depicts the resultant velocity for each test and Figure 2.6b displays the total displacement. Each test has a maximum velocity of the same order of magnitude ranging between 250-500mm/s and total displacements of 15-35mm. The results show that the thicker the slope (Loose 3), the more potential energy that can be transformed into kinetic energy, resulting in in a faster slide and larger amount of displacement, compared with Loose 4 (thinner).

The same analysis was performed on the four tests for two locations along the base (B1 and B2). The results are shown in Figure 2.7a and b. The patch located near the toe of the slope has similar velocity and displacement profiles as the single patch tracked in Figure 2.6a. However, it can be seen in Figure 2.7a I-IV that the patch farther along the base experiences a lower maximum velocity and a delay in the spike of velocity values. This time offset is expected as the farther field locations await the propagation of the shearing front. Accordingly, displacement of patch B2 farther along the slope base is also delayed. Of importance from both Figure 2.6 and Figure 2.7 is that the magnitude of the velocity for each failure is similar for each test. These velocities are the speed at which the slope experiences shearing. It can also be seen from both Figure 2.6 and Figure 2.7 that there is noise within the data. This noise is attributed to erroneous tracking of patches during analysis, however, there is a clear trend with the results. By studying

individual patches at different locations along the model, it is shown that areas farther away from the initial event experience decreasing amounts of displacement and velocity.

However, just as tracking DIC patches along the base gives us the capability of quantifying the velocity of landslide movement it also allows for us to determine the velocity of shear propagation through the model. Given the large number of PPTs imbedded in the model, the velocity of the liquefaction front can also be quantified and compared to the velocity of the shearing propagation. Figure 2.8a and b show DIC and PPT results from Test L1 for three locations along the base of the landslide.

As expected, there are time offsets between the three locations, as each location awaits the arrival of the propagation front. It can be difficult to consistently determine the time at which a patch begins displacing and when the PPT begins experiencing the generation of excess PWP. Therefore, a defined threshold value was selected. This threshold was chosen to be the point at which 20% of the maximum resultant displacement and maximum excess PWP has been exceeded, defined hereafter as t_{20}. This threshold value enables a consistent method for determining the time at which deformation and excess PWP generation has 'started'. Values of t_{20} were selected for each DIC subset and PPT (Figure 2.8a and b). Plotted in Figure 2.9a and b are the t_{20} results for all four loose tests. In Figure 2.9a, the location for seven (7) patches are plotted against the time it took for the patches to reach the t_{20} ratio. In Figure 2.9b it is done for ten (10) PPTs located along the base of the model. Applying a line of best fit for each of these plots shows a linear relationship. Since rapid shearing of a loose saturated soil generates excess PWP, it is unsurprising to see that both plots show the same velocity of propagation through the model of ~ 4.2 – 4.3 m/s. Comparing this rate to the velocity of the initial failures (0.25 – 0.5 m/s) it can be seen that the propagation front travels at a velocity an order of magnitude larger than the initial failure. This shows that the velocity of propagation of a liquefaction front is not dependent on the velocity of the initial failure and travels through the model significantly faster. In these tests, the soil liquefied at a rate of ten times faster than the failure itself moved.

2.3.3 Dense Tests

The same procedure that was used to create the loose contractile soil tests and rising groundwater conditions was used to model two dense dilative tests. Groundwater flow was continuously increased to try and induce a liquefaction event; however, no such failure had yet been reached when the pumps reached their maximum flowrate. The final flow rates for the two dense tests were greater than that of all the loose tests (Table 2.1). Although no deformations were triggered during the application of a rising groundwater table, a DIC analysis was performed for both tests. The superimposed DIC data on still frame images from test Dense 1 (D1) are shown in Figure 2.10. It is evident from the plotted displacement vectors that no displacement was recorded during testing. Although these two tests did not experience liquefaction, there is evidence that erosion competed as a failure mechanism at these high flow rates. The original geometry in test D1 consisted of a sloping section and a flat horizontal base. From the photos in Figure 2.10 it is evident that the top surface of the base is no longer horizontal although it did not experience any movement due to shearing. Therefore, another form of failure mechanism, such as erosion, must have occurred in order to change the geometry. This demonstrates that these tests were truly dense of the critical state. If these tests had been sufficiently loose, it would be expected that a dilative failure would have occurred that would result in no liquefaction of the base.

2.4 Conclusions

The objective of this study was to investigate the speed of propagation of the liquefaction front within the soil at the base of a landslide in a simplified physical model. Four experiments with a loose contractile soil and two experiments with a dense dilative soil were performed in a geotechnical centrifuge using a dense sensor network of PWP sensors and high-speed imaging to capture the temporal and spatial distribution of excess PWPs and shearing within the soil mass. It was found that the loose tests all experienced liquefaction, whereas the dense tests did not. Instead, the dense tests were subject to a different competing failure mechanism of erosion. Image analysis of the loose tests, in which a localized toe failure was observed to shear and liquefy the soil at the base of the landslide, showed that the velocity

of the initial failure was an order of magnitude slower than the subsequent velocity of propagation of the liquefaction front. In other words, these experiments illustrate that the velocity of the expansion of the instantaneous front of the landslide due to liquefaction is not governed by the speed of the initial failure. Due to the limitations of the physical model, the liquefaction of the base stopped at the end of the model once there was no more soil to liquefy. It is therefore possible that the zone of liquefaction at the base of the landslide could have extended farther if the dimensions of the model were longer.

These observations have significant implications for the prediction of the maximum distal reach of landslides in which static liquefaction may play a role. Most dynamic models of landslide runout (e.g. DAN/W) are calibrated with rheological properties, such that the release of a soil volume on the topography matches the trimline of the observed failure, with entrainment only occurring under the sliding soil (McDougall, 2017). However, the experimental observations here indicate that the landslide front can expand at a velocity an order of magnitude higher than the initial failure – essentially liquefying the base soil in front, rather than simply underneath the initial toe failure. The observations indicate that additional work is required to capture this behavior within numerical models.

Furthermore, when considering landslide remediation options, it would be important for either a densification program to be implemented in order to densify the basal region or install a drainage system to be installed to control groundwater levels. Densifying the soil to a sufficient degree will make it so that any possible failure will be dilative, and controlling groundwater conditions will decrease the required water level so that any excess PWP will not lead to liquefaction.

2.5 References

Askarinejad, A., Beck, A., & Springman, S. M. (2014). Scaling law of static liquefaction mechanism in geocentrifuge and corresponding hydromechanical characterization of an unsaturated silty sand having a viscous pore fluid. Canadian Geotechnical Journal, 708-720.

Beddoe, A. R., & Take, W. A. (2016). Loss of slope support due to base liquefaction: comparison of 1g and centrifuge landslide flume experiments. Soils and Foundations, 251-264.

Iverson, R. M., George, D. L., Allstadt, K., Reid, M. E., Collins, B. D., Vallance, J. W., . . . Bower, J. B. (2015). Landslide mobility and hazards: implications fo the 2014 Oso disaster. Earth and Planetary Science Letters, 412, 197-208.

Keaton, J. R., Wartman, J., Anderson, S., Benoit, J., deLaChapelle, J., Gilbert, R., & Montgomery, D. R. (2014). The 22 March 2014 Oso Landslide, Snohomish County, Washington. National Science Foundation.

McDougall, S. (2017). 2014 Canadian Geotechnical Colloquium: Landslide runout analysis- current practice and challenges. Canadian Geotechnical Journal, 54 (5): 605-620.

Ng, C. W. (2008). Invited special lecture: Deformation and failure mechanisms of loose and dense fill slopes with and without soil nails. Proceedings of 10th International Symposium on Landslides and Engineered Slopes, (pp. 159-177). Xi'an.

Rezzoug, A., & Konig, D. (2004). Scaling Laws for Centrifuge Modeling of Capillary Rise in Sandy Soil. Journal of Geotechnical and Geoenvironmental Engineering, 615-620.

Take, W. A., & Beddoe, R. A. (2014). Base Liquefaction: a mechanism for shear-induced failure of loose granular slopes. Canadian Geotechnical Journal, 51(5): 496-507.

Take, W. A., & Beddoe, R. A. (2015). Physical modelling of rainfall-induced flow failures in loose granular soils. IOP Conference Series: Earth and Environmental Science.

Take, W. A., Beddoe, R. A., Davoodi-Bilesavar, R., & Phillips, R. (2015). Effect of antecedent groundwater conditions on the triggering of static liquefaction landslides. Landslides, 469-479.

Take, W. A., Bolton, M. D., Wong, P. C., & Yeung, F. J. (2004). Evaluation of landslide triggering mechanisms in model fill slopes. Landslides, 173-184.

White, D. J., Take, W. A., & Bolton, M. D. (2003). Soil deformation measurement using particle image velocimetry (PIV) and photogrammetry. Geotechnique, 53(7): 619-631.

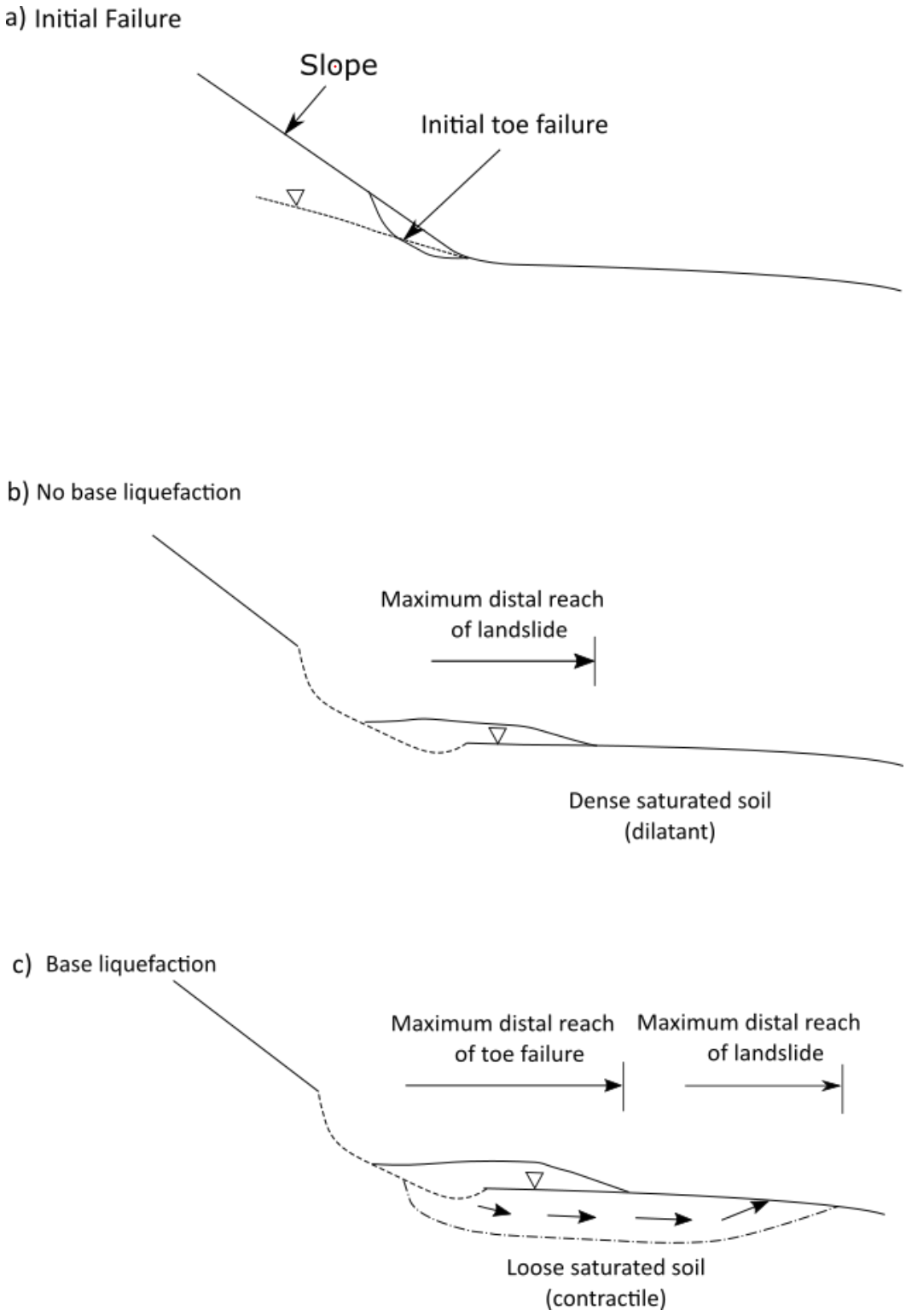

Figure 2.1 Effect of a small initial toe failure on the stability of the base of the slope. Image b) shows what the resultant landslide would be in a dense soil condition with the initial failure in a). Image c) shows the base failure in a loose contractile soil given events of a).

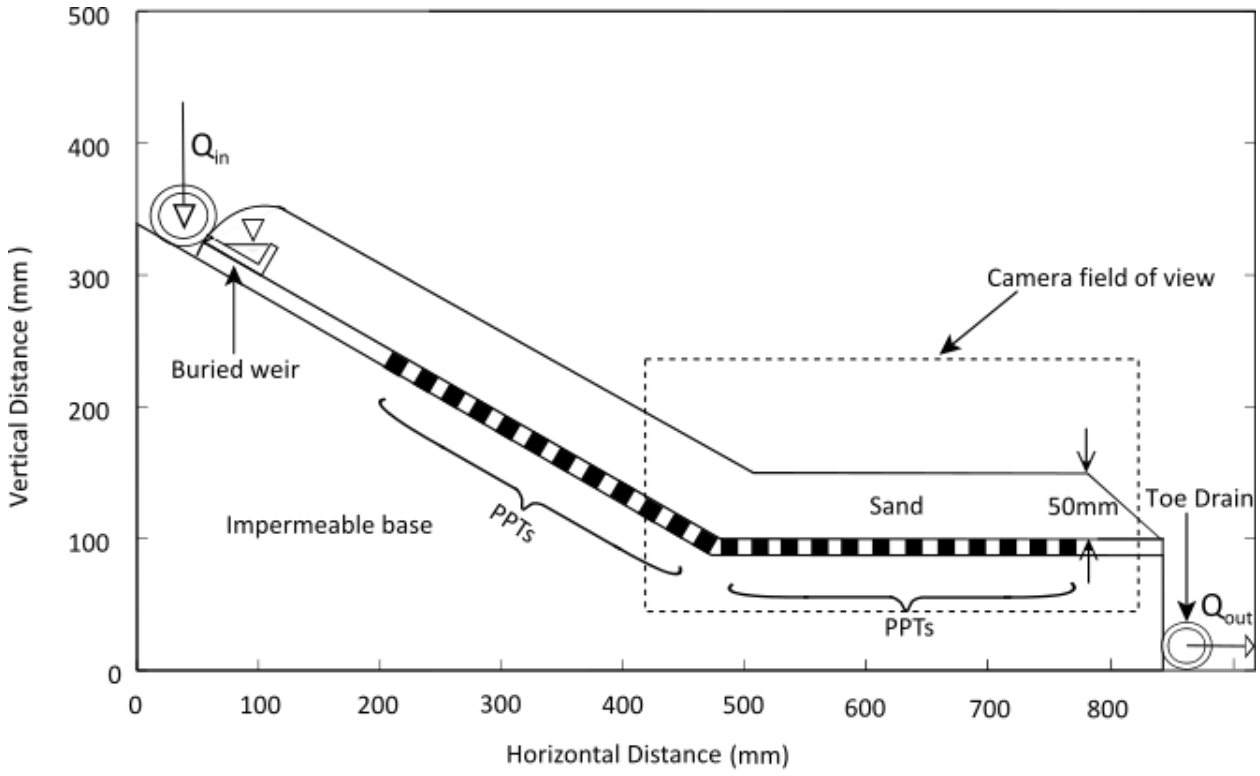

Figure 2.2 Geometry of the physical centrifuge model. Illustrated are various PPT locations, hydrological boundary conditions as well as the field of view of the high-speed camera.

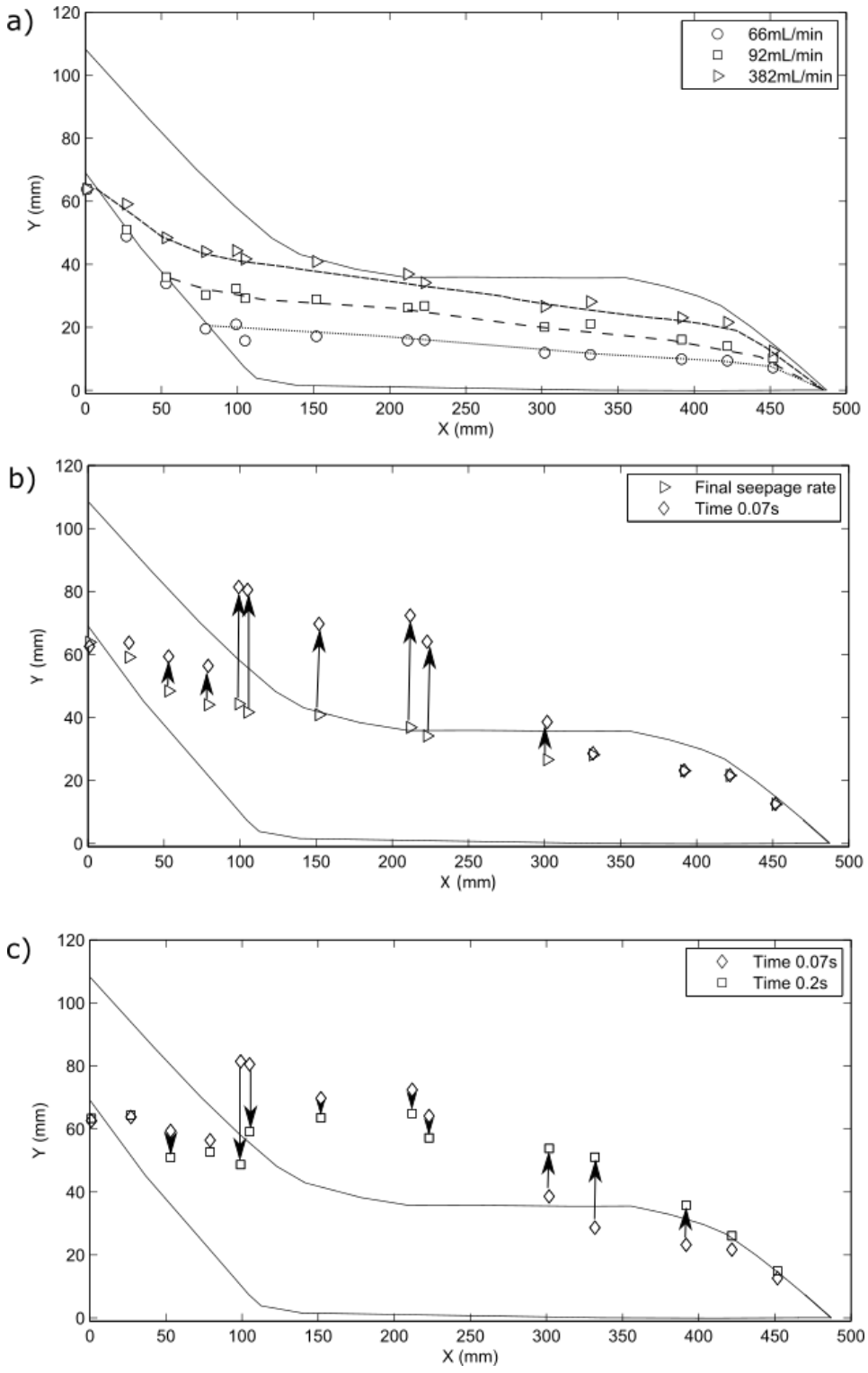

Figure 2.3 PWP response to an increase in groundwater table is shown in a). The flowrates for each plotted groundwater table are also shown in a). PPT response shortly after the initial failure is represented, 0.07s, in b) with c) showing PPT response after 0.2s.

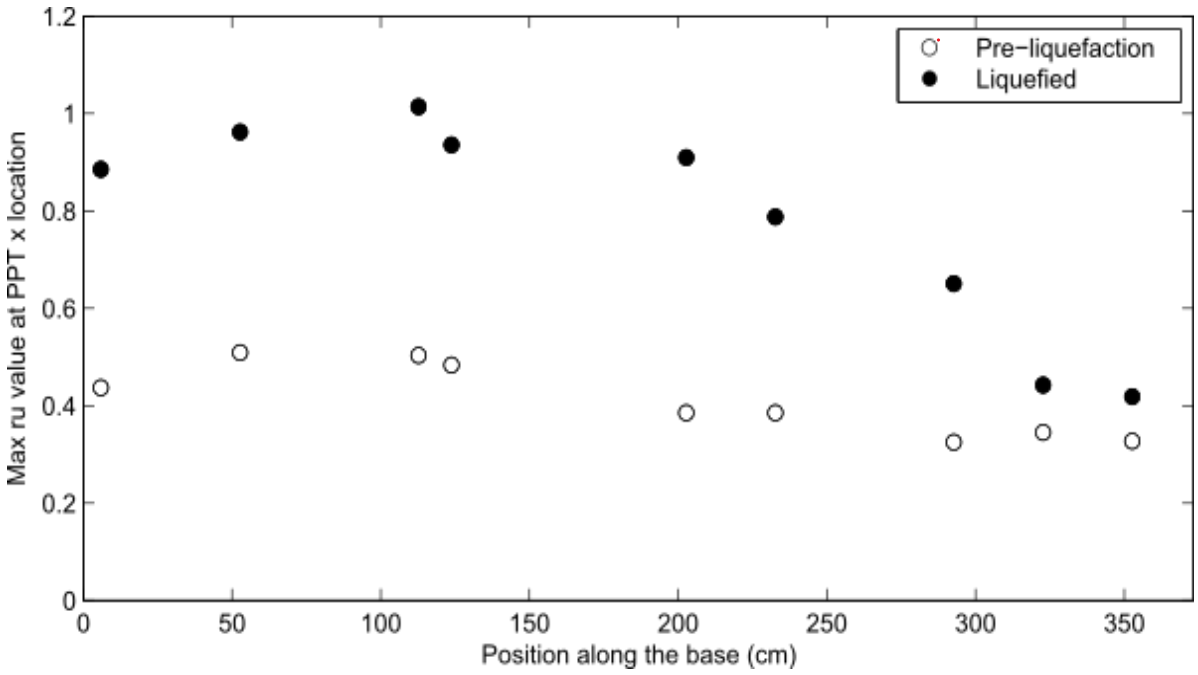

Figure 2.4 Values of maximum ru for Loose 1. The open circles represent maximum r_u values immediately before failure and the closed circles are for maximum r_u values during shearing.

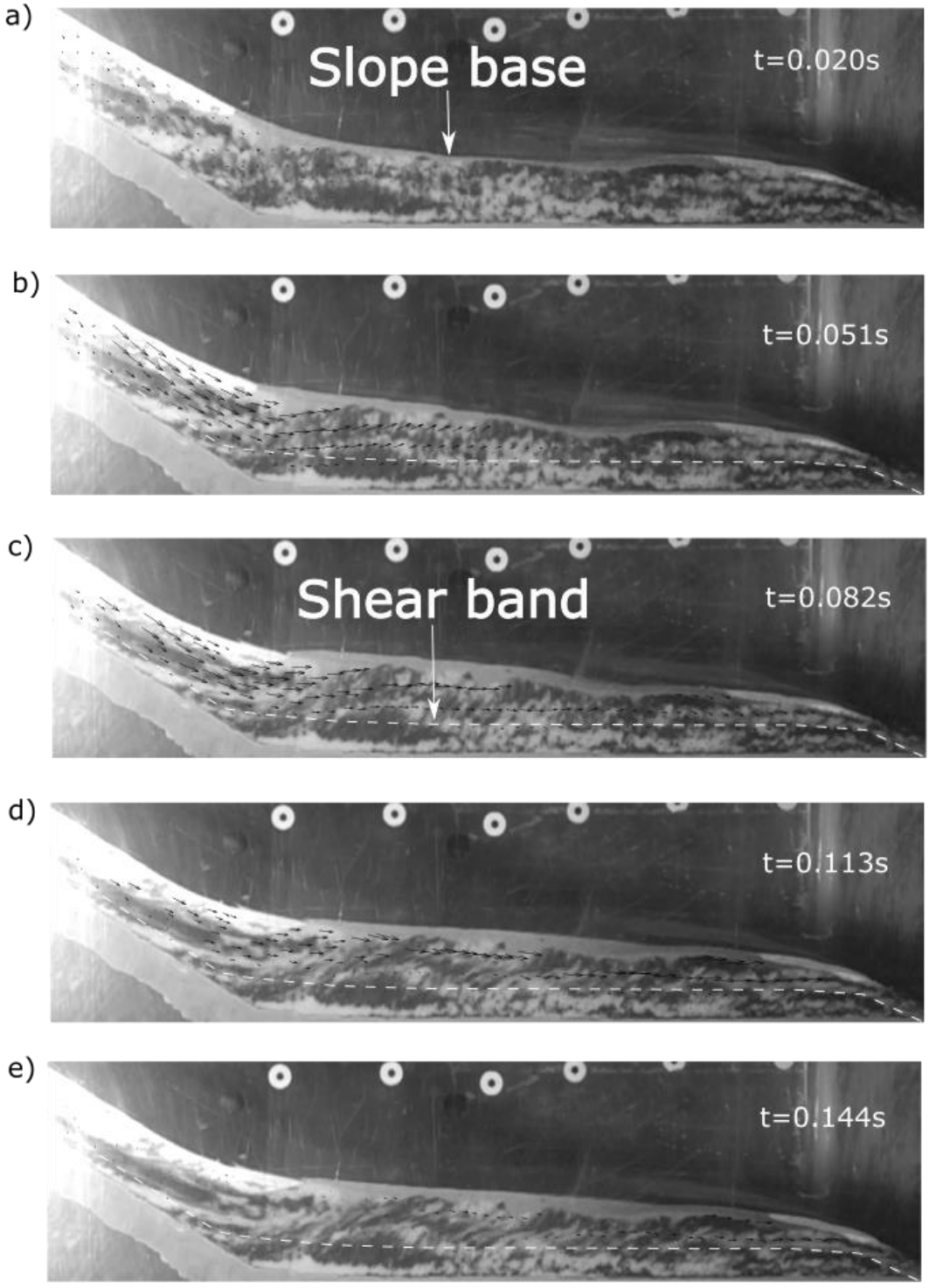

Figure 2.5 Vectors showing displacement over a period of 0.020s for each still frame. The images highlight the transient movement that occurs, starting with a small toe failure in a) and transitioning to a larger failure in b) and propagating farther along the base of the slope in c-e).

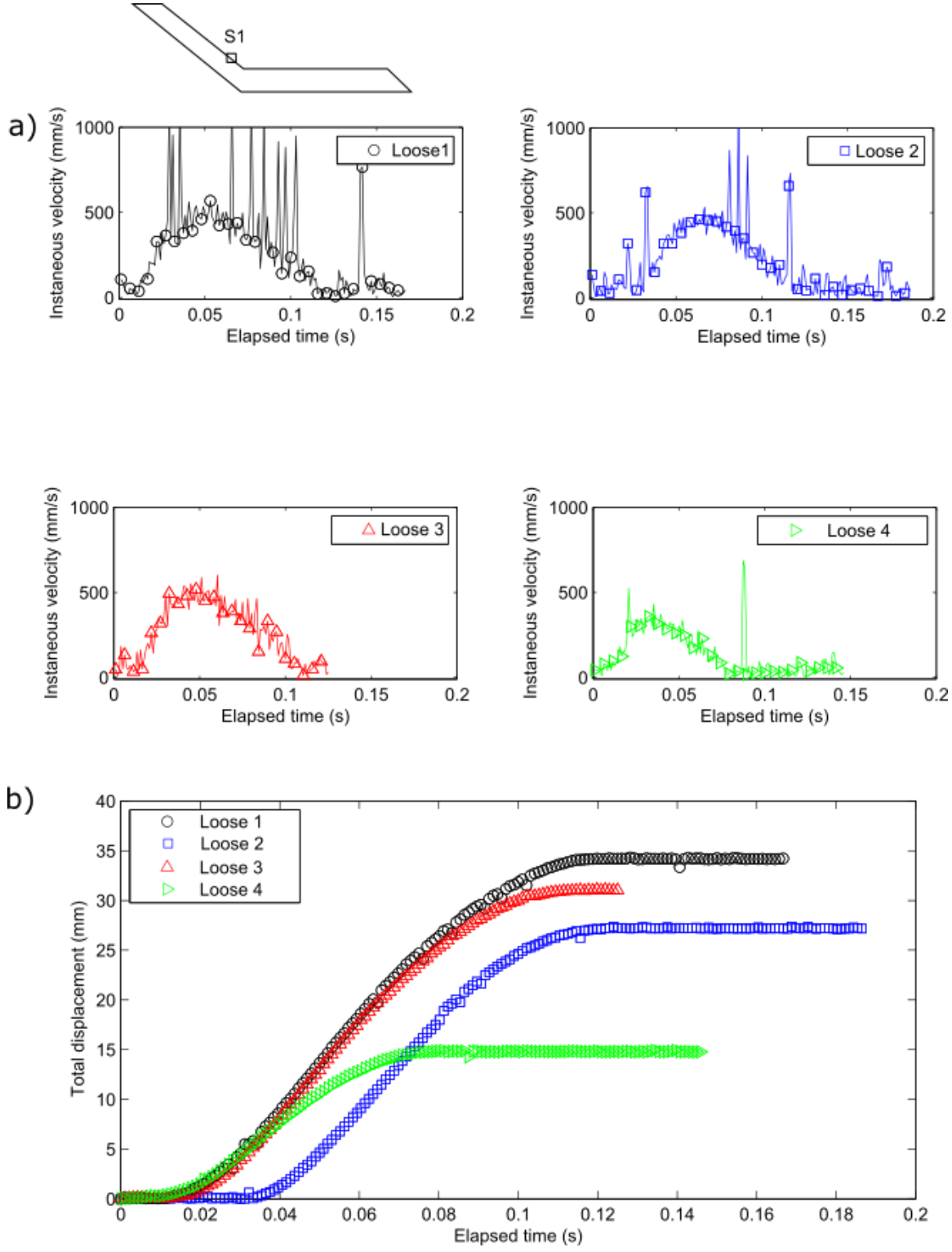

Figure 2.6 Section a) represents the instantaneous velocity of one DIC subset located in the initial shearing event. A representation of the location of the tracked patch is shown in the top left corner of the figure. Section b) displays the total displacement of that patch.

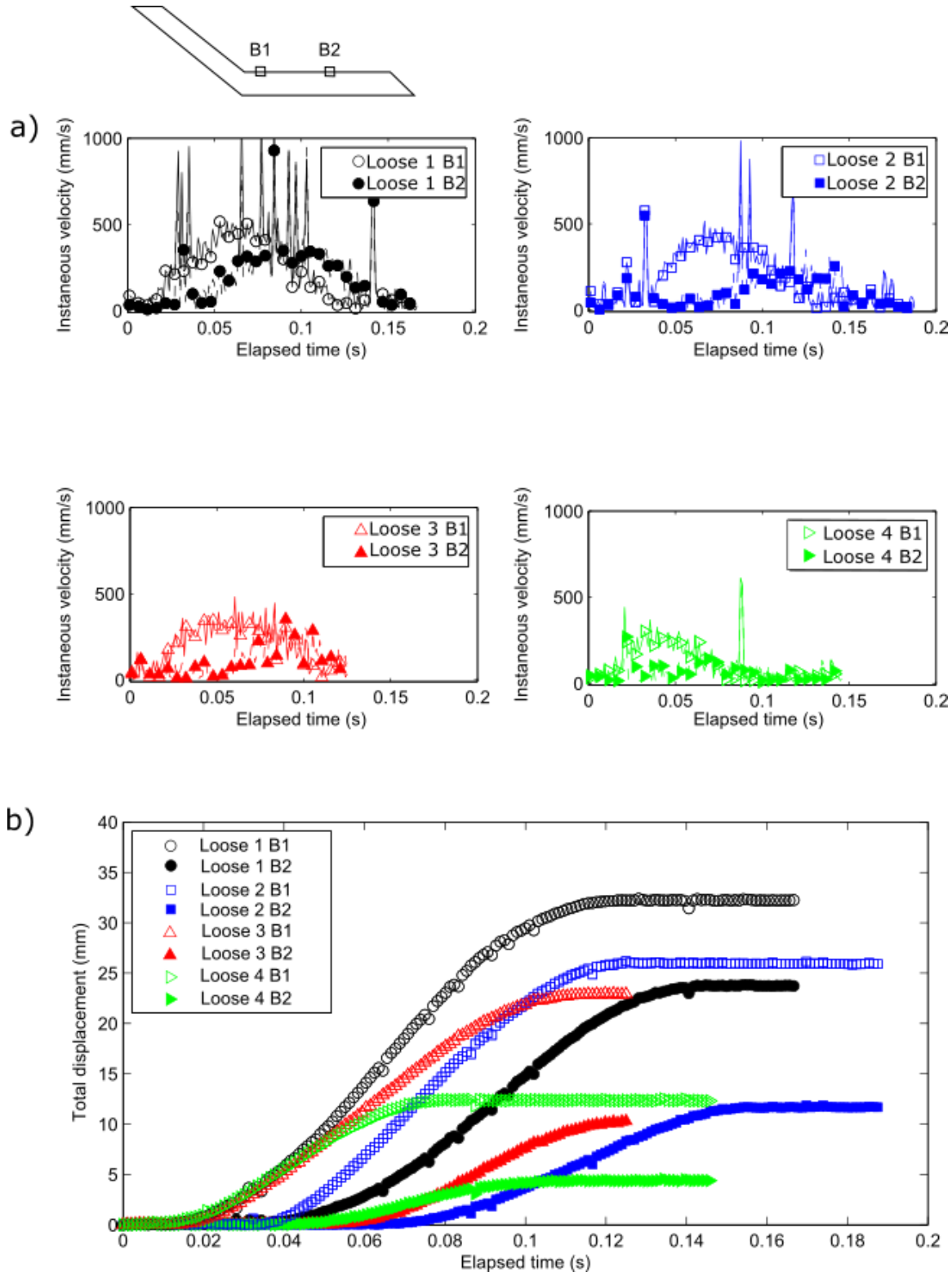

Figure 2.7 Sections a) and b) illustrate the instantaneous velocity and total displacement for two patches along the base.

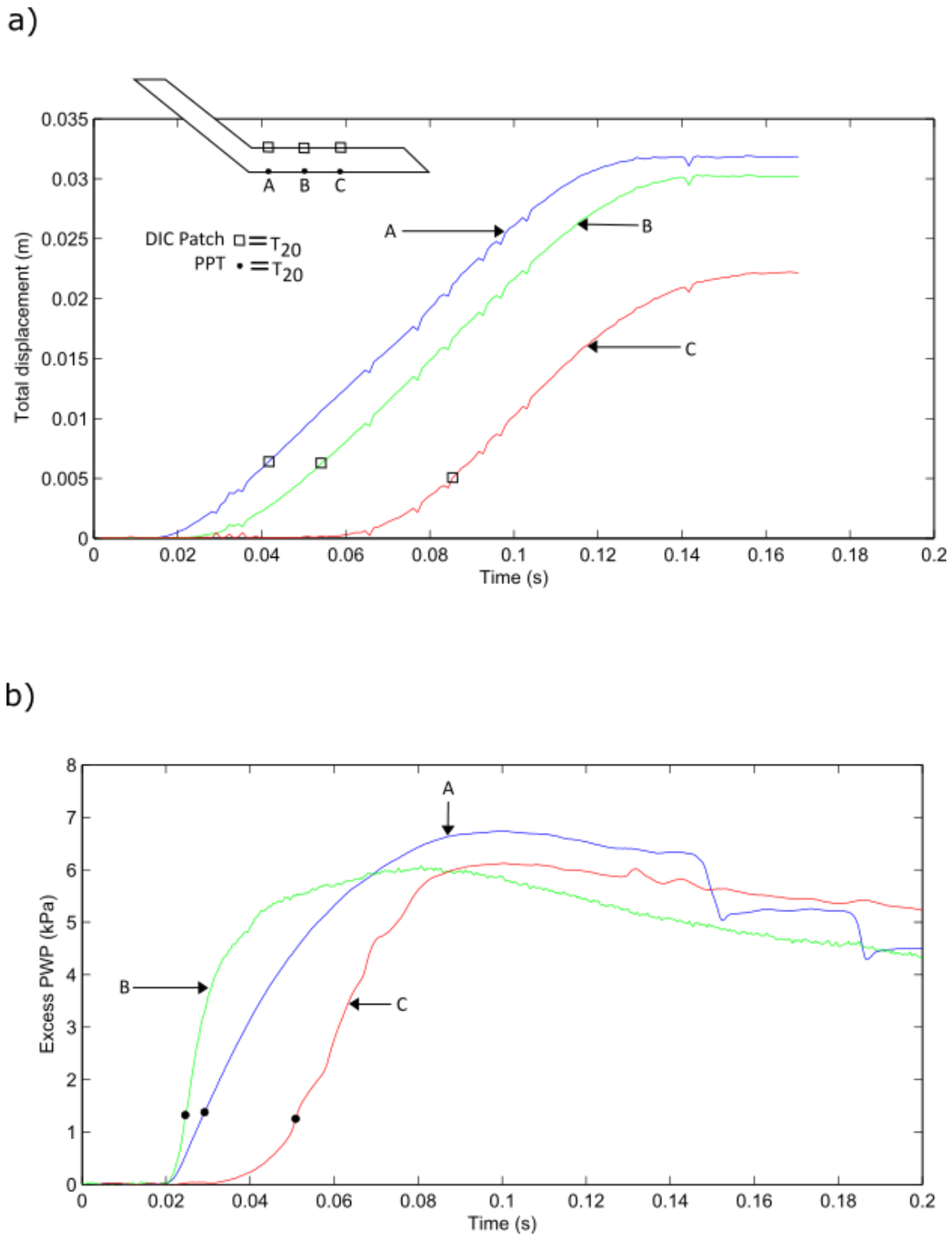

Figure 2.8 Results at three locations along the base of the model for test Loose 1 showing a) the total displacement, and b) the excess PWPs generated during shearing. The location of t_{20} for displacements and PWPs is also identified.

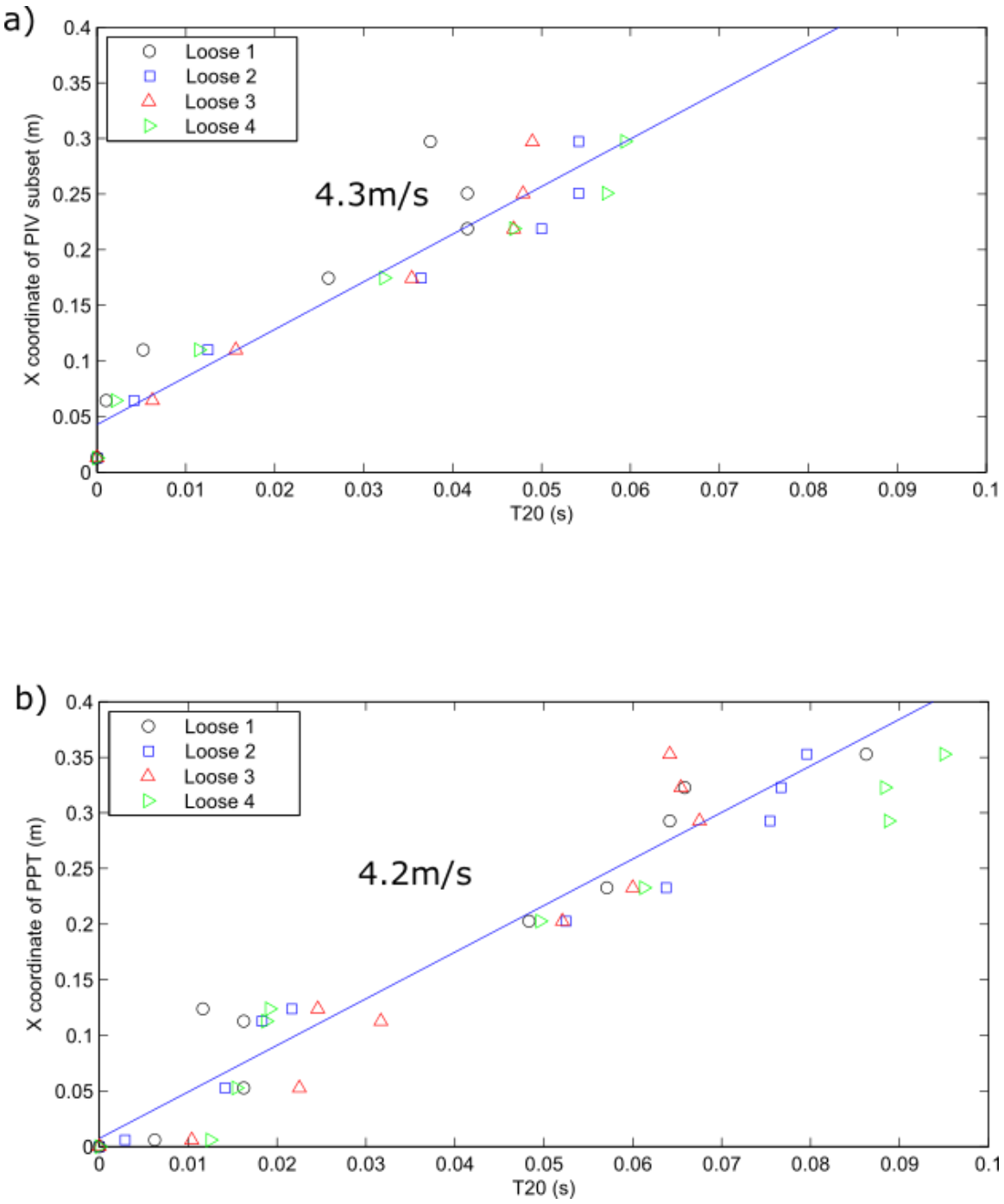

Figure 2.9 Plots of x locations for DIC subsets, a), and PPTs, b) versus t_{20}. Plots a) and b) represent the shearing and liquefaction propagation front respectively.

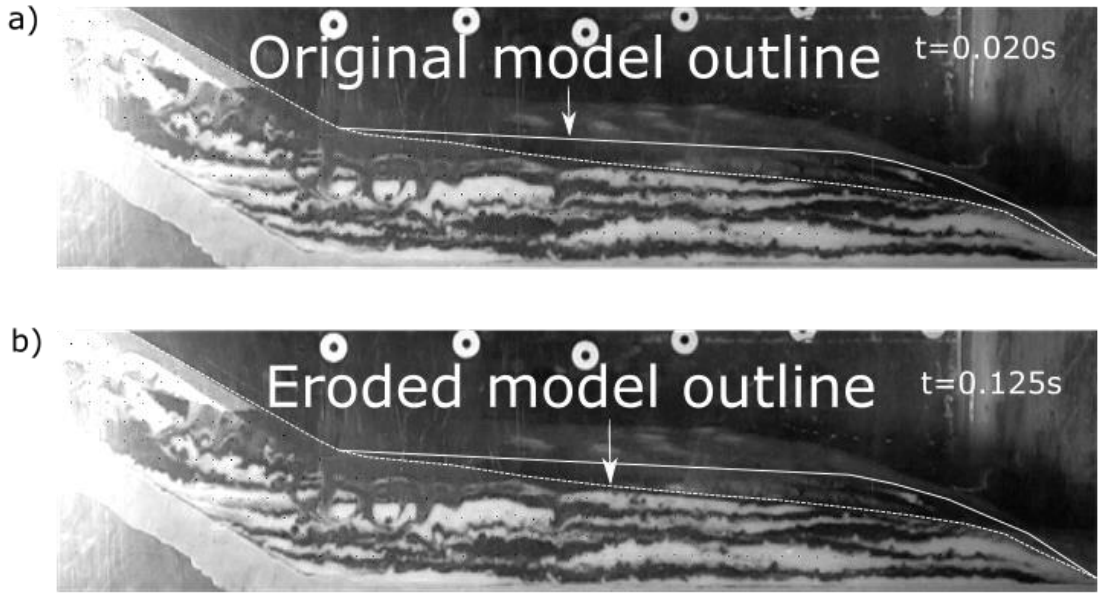

Figure 2.10 Two still frames with superimopsed images of vector displacement for test Dense 1. Image a) shows the displacement over a period of 0.020s from the start while image b) shows displacement over the same time period but from 0.105-0.125s. Also depicted are the outline of the model prior to satuartion of the material as well as the model outline post-erosion.

Chapter 3

Mobility of saturated granular material observed in inclined dam break experiments

3.1 Introduction

The management of landslide hazards requires a prediction of the likelihood of triggering a potential sliding mass as well as a prediction of the mobility of the resulting debris. Landslide mobility is a term often used to describe the flow characteristics of the debris; specifically, the velocity of the debris and the maximum distal reach of the final landslide deposit. PWP is known to play a significant role in defining the soil behavior observed within both of these processes. During triggering, it is well known that increases in pore pressure results in a reduction of effective stress. This in turn, decreases the shear strength of the soil along a potential failure surface, increasing the chances of slope instability. Once triggered, PWP can also have a significant impact on the mobility of the debris. Rapid shearing of loose soils within a landslide can lead to the generation of excess PWPs, which further reduces the soil shear strength and leads to increased velocity and distal reach. The potential magnitude of increased mobility due to the static liquefaction of the debris has recently been investigated experimentally by Take and Beddoe (2015), who triggered landslides in identical physical models of loose fine sand with varying antecedent groundwater levels. The results of this testing program illustrated that the process of static liquefaction made possible by high ground water levels prior to landslide triggering could result in a seven-fold increase in mobility over an identical model which did not experience liquefaction due to low groundwater levels prior to landsliding.

In current geotechnical practice, assessment of landslide triggering and mobility are typically conducted as separate analyses. Limit equilibrium analyses are often used to assess static stability, while shallow flow models for dynamic motion are conducted to predict mobility based on frictional or Voellmy

rheology (e.g McDougall, 2017). The majority of the literature pertaining to the physical modeling of landslide mobility has focused on dry flows (Savage, 1979, Hungr & Morgenstern, 1984, Bryant et al., 2014). Considerably less work has been conducted on the mobility of multiphase flows.

Shallow flow dynamic models typically incorporate PWP effects as r_u, which is defined as the ratio of pore pressure to the total stress at a point within the soil. Following the concept of effective stress, the basal shear resistance at this point along the plane of motion is therefore given by:

$$\tau_B = \sigma_v(1 - r_u)tan\varphi \qquad \text{Eq 3.1}$$

In this equation τ_B is the basal shear resistance, σ_v the total stress and φ represents the friction angle. From this Eq 3.1 it can be seen that increases in PWP directly increase r_u, resulting in a correspondingly linear reduction in available basal shear strength. Given a decrease in basal shear strength, it would be expected that saturated flows would exhibit higher mobility than dry flows of identical source volumes under the same boundary conditions.

Conducting granular dam break experiments, in which a block of granular material is instantaneously released from the top of an incline, provides a useful mechanism to investigate the fundamental shearing behavior of saturated granular flows under controlled experimental conditions. In particular, the particle size of the granular material will affect its permeability and therefore its unsaturated shear resistance and its rate of pore pressure dissipation, should the flow experience partial drainage during the time scale of flow duration. As the particle size of the granular material increases the size of the flume used for testing also needs to increase. The flume size used must be large enough to test a representative volume of material. Bryant et al. (2014) has developed a large-scale landslide testing flume at Queen's University. Use of this flume allows for large scale testing of granular material with different source volumes and varying grain sizes. The objective of this chapter is to investigate the shear behavior of saturated granular material of different particle sizes observed within inclined dam break experiments. Specifically, experiments will be conducted releasing identical source volumes of 3 mm and 0.12 mm diameter grains

to: a) identify the experimental challenges associated with boundary conditions and instrumentation required to test these materials; b) develop experimental techniques for testing saturated granular materials; and, c) provide preliminary experimental observations of the influence of particle size on the mobility of saturated granular materials upon which a large-scale experimental program could be designed and conducted in the future.

3.2 Methods

3.2.1 Flume

The Queen's University landslide flume was used to conduct multiple dam break experiments of various grain sizes. The flume channel has dimensions of 2.09 m in width and 8.23 m along the sloped section which is fixed at an angle of 30^{o} from the horizontal. At the toe of the sloped section there is a 36 m long runout section. The base of the flume is aluminum and is coated with a textured paint to enhance basal friction. The sidewalls of the flume are comprised of panes of tempered glass 19 mm in thickness and 1.21 m in height (e.g. Take et al., 2015, Coombs et al., 2018).

At the top of the sloped section of the flume is a soil release box. This box was filled with various volumes of granular material prior to testing. This release box has internal dimensions of 1.75 m in width, 1.5 m in length and 0.75m in height perpendicular to the slope, resulting in a maximum volume of 1.68 m^3 (Bryant et al., 2014, Coombs & Take, 2018).

In order to saturate the granular material a Pentair 3HP IntelliFLO Variable Speed Pump was used to transport water from a tank at ground level to the top elevation of the release box (Bullard et al., 2018). For the fine sand, water was added to the release box prior to the addition of granular material. This was in an effort to completely saturate the material. As for the coarse grained material, water was added after the granular material had been loaded into the release box. The high porosity and permeability of the coarse grained material readily enabled the saturation of the material. Figure 3.1 shows a schematic of the flume and soil release box with a test volume of 0.4 m^3.

Movement of the release box door is controlled by double-acting pneumatic actuators. When a source volume is added to the release box, the actuators counteract the pressure exerted by the soil. Reversing the actuator pressure opens the release box at ~1 m/s allowing the contained granular material to flow downslope (Coombs & Take, 2018)

3.2.2 Granular Material

Two granular materials of different particle sizes and rheology were used for the dam break scenarios. Three of the tests were conducted using spherical ceramic beads (Denstone 2000 Support Media) produced by Saint-Gobain NorPro. The granular material possesses an average diameter of 3 mm and a dry bulk density of 1400 kg/m^3 as measured by Coombs and Take (2018).

Additional tests with fine sand were also conducted using #730 Silica Sand by Weldon Company with an average grain size of 0.12 mm. The soil release box was flooded with water and the fine sand was slowly added into the flooded container using an automated dumping bucket to ensure saturation. Once the source volume of material had been loaded into the release box, the door was opened and the triangular wedge of soil was allowed to flow downslope.

3.2.3 Instrumentation

Multiple PPTs and cameras were installed along the length of the flume to characterize the downslope flow of the granular material. Thirteen (13) Motorola MPX5050GP PPTs were installed along the flume and were used to capture the change in pore pressure. As the mobile granular mass traveled overtop of the opening of each sensor, readings were taken at a sampling at a rate of 100 Hz. Seven (7) PPTs were located along the sloped section of the flume in the middle with the remaining (6) along the middle of the base. The strategy for installing PPTs along both the slope and base was adopted to attempt to observe the change in basal pore pressure as the mobile mass transitioned from the sloping section to the horizontal flume base. PPT measurements would also enable a comparison to be made between the pore pressures

expressed as total heads and the thickness of the saturated granular flow as measured from videos recorded using the cameras.

The type of camera used for this testing was the Sony RX10M2. Two cameras were utilized during each test, and they recorded the mobile flow at a rate of 480 frames per second with a resolution of 1920x1080 pixels. One camera was situated parallel to the sidewall, mounted on a tripod, and the other mounted to an overhead cross brace aimed perpendicular to the flume slope. The two camera positions were located 6.17 m and 6.23 m downslope of the release box for the cross brace and tripod mounted cameras, respectively (Coombs & Take, 2018). The camera positions were chosen to in order to record flow data at the farthest location from the release of the source material and prior to the flow contacting the horizontal section. A Pallite VIII flicker-free light was used to illuminate the area of interest.

The video files recorded during the tests were used to quantify both the sidewall thickness and the velocity of the flowing material. Digital Image Correlation (DIC) was used to track the flow through time from frame to frame which allows the calculation of flow velocity. The GeoPIV program developed by White et al. (2003) was used for the analysis portion of this experimental program. This program allows a user to define a specific set of pixel patches to quantify soil deformations. Through the use of a static mesh, GeoPIV provides results of displacements of subsets from image to image. The displacement of particles in each patch is correlated by comparing the pixel intensity of each patch. Using a known scale factor, reported pixel displacements can be converted into real-space measurements and used to quantify flow velocity and thickness. The camera situated parallel to the viewing glass was used to determine the sidewall flow thickness while the overhead camera was used to determine the velocity in the middle of the flowing mass.

Once the flowing mass had come to rest along the base section of the flume a terrestrial LiDar scanner was used to collect information on the resultant deposit shape. For each test a scan was taken from two different positions with a FARO Focus8 Laser Scanner. Scanning from the two locations enabled the scanner to capture the entirety of the deposit morphology. Scans were used to determine both the centre of

mass as well as the distal reach of the deposit. With this information, a comparison can be made between the travel angle (α_g) and the Fahrböschung angle (α) (Heim, 1932). The travel angle is a measure of the inverse tangent between a source volume's centre of mass and the centre of mass of the flow deposit (Okura et al., 2000). The travel angle allows for a quantification of where the majority of the source volume will be located upon mobilization of the material, which can be useful in a risk analysis approach; however it does not give any indication of the extent of the impact zone. The Fahrböschung angle measures the inverse tangent of the location of the release point at the head scarp of the source with respect to the location of the distal reach of the deposit. Analysis using the Fahrböschung angle allows for a quantification of the extent of impact (i.e. this parameter also includes the effect of increased spreading of the debris).

3.3 Results

3.3.1 Coarse Grained Soil Test Results

Three tests consisting of 3 mm diameter particles were conducted using the Queen's University Landslide Flume. The three tests were of different source volumes of 0.2 m^3, 0.4 m^3, 0.7 m^3 and each was fully saturated. A test with a source volume of 0.4 m^3 using the same granular material was also conducted by Coombs and Take (2018), in a dry state. Comparisons can therefore be made between the resultant mobilities of the dry and saturated flows and their deposit morphologies. Results of side wall velocity measured in both of these 0.4 m^3 source volume tests are shown in Figure 3.2. It is evident from Figure 3.2 that both the saturated and dry granular flows have the same initial velocity of ~5.4 m/s; however, 1 s into the flow sequence, the velocities of both tests begin to diverge. The wet mass clearly experiences a decline in velocity at a must faster rate than the dry mass. This can be attributed to the influence that saturation of the source volume has on the mobility of the flow. Saturating the soil reduces the basal shearing resistance, resulting in a high mobility flow in comparison to the dry material. At 2.5 s, the velocity of the saturated mass stabilizes at ~0.5 m/s indicating that the majority of the flowing mass has

passed in this time. In comparison, the dry material still has a velocity above 3 m/s at 3 s into the flow. Given that the velocity at this time is still relatively high, it can be assumed that the data does not represent the entirety of the flow. The fact that the entire flow was not captured within a 3 s period while the entirety of the saturated flow was captured in a shorter time frame adds to the validity of the hypothesis that the saturated flow was more mobile.

Another way of quantifying the mobility of a saturated versus dry flow is by comparing the resultant deposit morphologies. If a flow has a higher mobility the maximum distal reach of the deposit will be farther away from the origin of the source volume. Figure 3.3 represents the resultant deposit shapes for the saturated and dry 0.4 m^3 tests. The "+" sign represents the centre of mass of the respective deposit. It can be seen that the dry mass has a roughly symmetrical deposit shape resulting in a centre of mass near the midpoint of the deposit. In contrast, the saturated mass has a right-skewed deposit shape. The skewness of the deposit results in a centre of mass farther along the flume base. Determining the centre of mass of the two deposits and the maximum distal reach of both tests enables the travel angles and the Fahrböschung angles to be determined. Comparing the travel angle of the two tests reveals that there is a difference of 2.7^o (a 9.8% difference). As expected, the saturated test has a lower travel angle than the dry tests, indicating higher flow mobility. When comparing the difference in the Fahrböschung angle, the evidence of the increased mobility of the saturated flow is again exemplified. The difference between the two Fahrböschung angles is 3.7^o (a 14.8% difference). It is clear from both methods of flow mobility quantification that the saturated flow resulted in a higher mobility flow than the dry test due to the decrease in shear resistance.

Knowing that saturating the granular material results in a higher mobility, a comparison of mobility can then be made between saturated tests of the same material with differing source volumes. The three source volumes were 0.2 m^3, 0.4 m^3, 0.7 m^3. Figure 3.4 displays the velocity results for the three tests. It can be seen that all three tests have the same velocity profile with different initial velocity measurements. As the source volume is increased, the initial velocity measurements correspondingly increase. The larger

velocities can be attributed to the fact that the larger source volumes have a greater gravitational potential energy. Increasing the source volume also increases the duration of time over which the flow event occurs. There is ~0.5s change in flow times between the 0.2 and 0.7 m^3 tests. Although the larger volume results in a faster velocity, the time it takes for the entirety of the mass to come to rest is longer than that of the smaller volumes due to the fact that a larger volume has to be transported. When looking at Figure 3.5, which represents the side wall thickness profile of the three tests, it can be seen that the thickness of the flow corresponds with velocity at the same time. Each test has a section of erratic data within the first 0.5s. This erratic data is from the leading edge of the flow which is dominated by collisional flow rather than frictional flow. As the flow progresses, it becomes increasingly more frictional and the thickness of each test decreases at a rate comparable to that of the velocity profile. This is continuing evidence that an increase in source volume equates to an increase in flow mobility.

As before, we can also compare the final deposit morphology of each test to quantify the mobility of each flow. From Figure 3.6, it is evident that a larger source volume travels farther than a smaller one. The largest volume of 0.7 m^3 traveled more than 2.5 times farther than the smallest volume of 0.2 m^3. A summary of the mobility of each flow is summarized in Figure 3.7. As the volume of the flowing mass increases, the resultant angular measures of mobility decrease, representing an increase in the mobility of the mass. Increases in mobility with increased source volume can be attributed to the entrained water content within the flowing mass. Referring to Equation 3.1, the variable r_u does not remain constant and can vary over the duration of the time of flow. With each increase in source volume, the thickness of the flowing mass correspondingly increases. The increase in flow thickness effectively increases the drainage path distance from the basal shear surface to the free surface at the top of the flow. The longer the water is trapped within the flow, the longer the basal shear resistance is suppressed, resulting in a more mobile flow.

It is clear that the presence of water in a coarse grained source volume enhanced the mobility of the resultant flow. To quantify the role that PWPs played in the mobility of the flow, PPTs were installed

along the midsection of the flume to capture the flow profile. Unfortunately, the pressure profile was more difficult to capture than expected. Results from the PPTs from the 0.7 m^3 test positioned along the slope can be seen in Figure 3.8. It can be seen that some of the PPTs respond accordingly to the pressure exerted upon them, while others experience either an apparent suction, or remain unresponsive. For the PPTs that do respond, it is difficult to determine an accurate reading based on the noise of the data. These results indicate that additional experimental work is required to investigate techniques for the measurement of basal fluid pressure along the shear surface. In particular, each sensor was attached to the base of the flume using approximately 50 mm of flexible tubing. It is possible that small volumetric changes within this tubing or the presence of small trapped air bubbles could have influenced the dynamic pressure recorded by the sensor. With both of these potential hypotheses, future testing should focus on minimizing the water reservoir within the sensor system. Furthermore, care must be exercised to eliminate any local disturbance in the surface roughness of the base of the flume at the pore pressure measurement point to eliminate local vortices that may influence the pressure recorded. This work has highlighted that further investigation into the measurement of PWPs in this scenario is needed. Despite the inability to collect quantifiable PWP data during this exploratory experimental program, it is still evident that water plays a large role in the mobility of coarse grained flow.

3.3.2 Fine Sand Test Results

Having observed the effect of pore water on the mobility of coarse grained materials, the second phase of the experimental work investigated the effect of particle diameter by replicating the experiment with a saturated fine sand. In an effort to achieve a loose granular configuration that would contract upon shearing, moistened sand was dumped into the release box which was previously filled with water. This strategy of pluviation of sand into water leads to the soil reaching terminal velocity as it falls, thereby ensuring a loose configuration as well as complete saturation of the soil. The first test that was conducted had a source volume of 0.5 m^3. Upon opening the release door, the free-standing water rushed out and the front face of the soil slumped. Figure 3.9 and Figure 3.10 depict the results of this test. It had been

expected that releasing the door would cause the soil to shear under its self-weight and if the soil was sufficiently loose and saturated, this would lead to a static liquefaction event. Assuming that the soil was too dense to be contractile, additional tests were conducted in which a concrete vibrator was used to liquefy the soil *in situ* before release. These tests were also conducted with a greater volume than the initial 0.5 m^3. It was hoped that increasing the volume would increase the likelihood that the soil would shear under self-weight. Once again, upon opening the release door, the soil remained within the box. It appeared that the concrete vibrator temporarily liquefied the soil but on removal of the device had actually lead to the densification of the soil and made it more dilative.

This series of tests proves that it is surprisingly difficult to generate a liquefaction event in a dam break experiment with fine sand. Further research is required to develop experimental techniques to ensure the soil is sufficiently loose to create contractile soil conditions. If the soil is loose enough, there will be a generation of excess PWPs upon shearing, which will lead to the liquefaction of the soil and create a high mobility flow. If the opposite is true, and the soil is dense, the soil will experience dilation upon shearing, and experience deformation but not flow failure. It is proposed that an upward hydraulic gradient system be developed to pre-liquefy the soil to ensure full saturation and a loose state upon sedimentation after the upward hydraulic gradient boundary condition is removed. Secondly, it is possible that the fluid phase is released from the source volume at the door faster than the solid fraction. Such a drainage front would be sufficient to create unsaturated conditions within the soil mass and develop matric suctions that could lead to increased shear strength. Further research is required to investigate whether this hypothesis has validity.

3.4 Conclusions

The objective of this chapter was to investigate the shear behavior of saturated granular material of different particle sizes observed within inclined dam break experiments. Experiments were performed by releasing a known source volume of 3 mm and 0.12 mm diameter grains using the Queen's University

landslide flume. These experiments were conducted with the following objectives: a) to identify challenges associated with boundary conditions and instrumentation required to test these materials; b) to develop experimental techniques for testing saturated granular materials; and, c) to provide experimental observations on the influence of particle size on the mobility of saturated granular material to facilitate the development of a large-scale testing program for future work.

To quantify the mobility of the coarse grained flow, high-speed cameras were used to measure the thickness and velocity profiles of three different tests. The three tests had source volumes of 0.2, 0.4 and 0.7 m^3. It was found that increasing the source volume lead to an increase in flow velocity, representing a higher degree of mobility. The resultant deposit morphology for each test was recorded using a terrestrial LiDar scanner. Analysis of the deposits showed that both the travel angle and Fahrböschung angle decrease with increasing source volume. This helps solidify the hypothesis that increasing source volume correspondingly increases the flow mobility.

It was clear from the testing that the addition of water to a granular material increases the flow mobility, as exemplified by the comparison between a dry and saturated flow of the same volume. PPTs were installed in the flume with the hope of recording the PWP of the flowing mass. This data is required to conclusively say what effect the water has on the mobility of the transient nature of the flow. Unfortunately, the data collected from the sensors was excessively noisy for a proper analysis to be conducted. Future recommendations for this type of testing would be to acquire sensors that can reliably capture PWP readings. In addition, future testing should focus on minimizing the water reservoir within the sensor system to reduce the possibility of small volumetric changes in the system that could lead to erroneous PWP data. Once the PPT issue has been resolved, further testing should be done where the source volume remains constant, but the degree of saturation changes with each test. Doing this would allow for determination of whether or not flow mobility increases proportionally with increasing water content.

Testing of a saturated fine sand emphasized the fact that dam breach experiments with this material can be difficult to conduct. Multiple tests were conducted to try to create a highly mobile flow. Each test resulted in a soil mass that dilated upon shearing. Attempts were made to pre-liquefy the soil via use of a concrete vibrator; however this appeared to have the opposite result and densified the soil. When conducting these tests in the future, special care should be taken to construct the model so that the soil is loose and contractile. One possible way of doing this would be to have a sieve that the soil passes through immediately after the sedimentation of the soil into the release box. Another suggestion would be to install a type of upward hydraulic gradient system that would liquefy the soil from the bottom up prior to removal of the hydraulic boundary condition.

3.5 References

Bryant, S. K., Take, W. A., & Bowman, E. T. (2014). Observations of grain-scale interactions and simulation of dry granular flows in a large-scale flume. *Canadian Geotechnical Jounral*, 52 (5), 683-655.

Bullard, G. K., Take, W. A., & Mulligan, R. P. (2018). Wave characteristics of tsunamis generated by landslides of varying size and mobility (Unpublished Doctoral Thesis). Queen's University.

Coombs, S. P., & Take, W. A. (2018). Physcial investigation of the flow structure and mobility behavious of collisional granular landslides (Unpublished Master's Thesis). Queen's University.

Heim, A. (1932). Bergsturz und Menschenleben. [Landslides and human lives.] Translated by N. Skermer. Vancouver, 1989: Bitech Press.

Hungr, O., & Morgenstern, N. R. (1984). Experiments on the flow behaviour of granular materials at high velocity in an open channel. *Geotechnique*, 34(3): 405-413.

McDougall, S. (2017). 2014 Canadian Geotechnical Colloquium: Landslide runout analysis- current practice and challenges. *Canadian Geotechnical Journal*, 54 (5): 605-620.

Okura, Y., Kithara, D., & Sammori, T. (2000). Fluidization in dry landslides. *Engineering Geology*, 56: 347-360.

Savage, S. (1979). Gravity flow of cohesionless granular materials in chutes and channels. *Journal of Fluid Mechanics*, 92: 53-96.

Take, A., Bowman, E., & Bryant, S. (2015). Physical modelling of granular flows at multiple-scales and stress levels. EGU General Assembly Conference Abstracts 17. Vienna.

Take, W. A., & Beddoe, R. A. (2015). Physical modelling of rainfall-induced flow failures in loose granular soils. *IOP Conference Series: Earth and Environmental Science*.

White, D. J., Take, W. A., & Bolton, M. D. (2003). Soil deformation measurement using particle image velocimetry (PIV) and photogrammetry. *Geotechnique*, 53(7): 619-631.

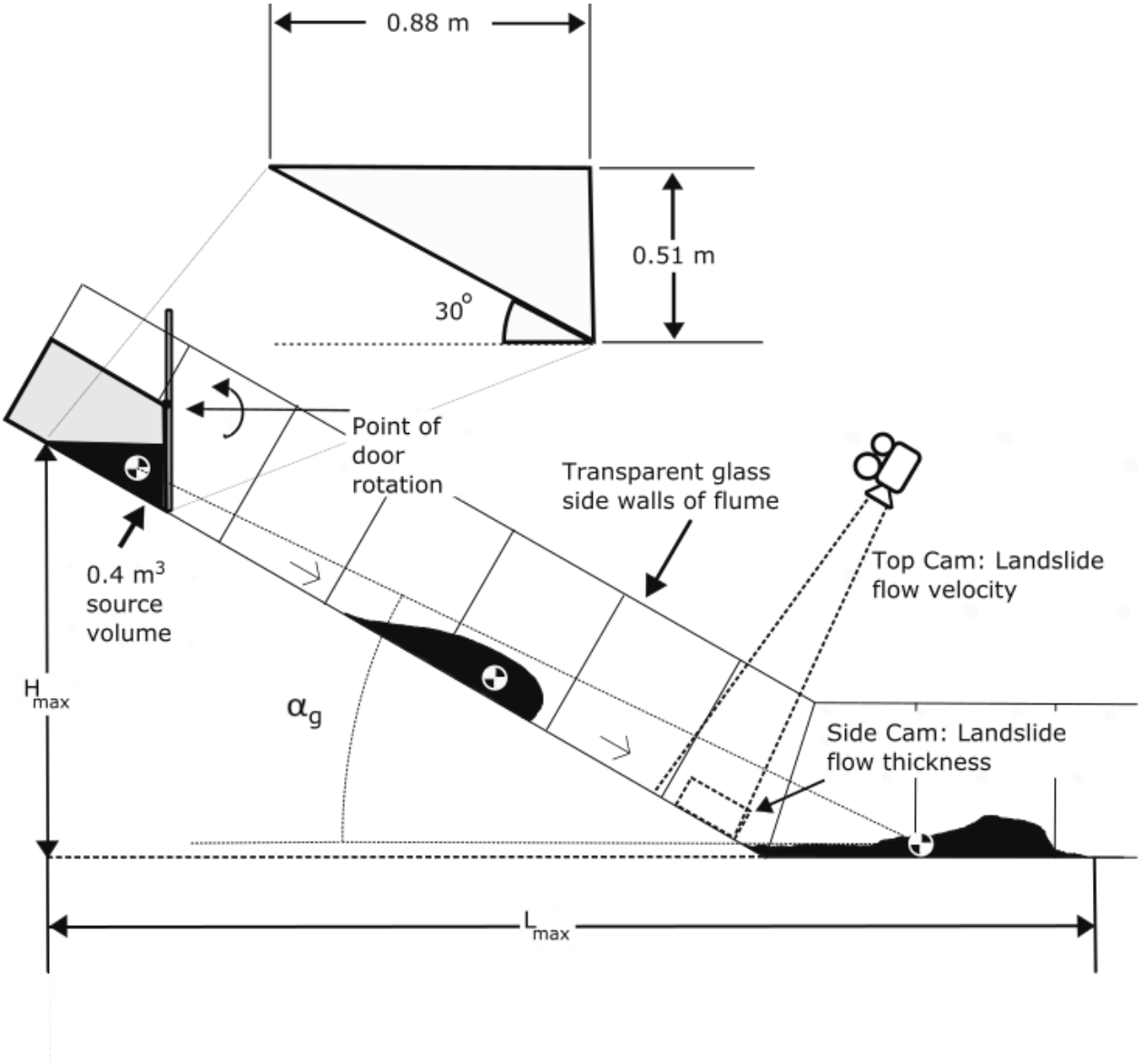

Figure 3.1 An illustration of the Queen's University Landslide flume. Camera viewing locations are also indicated along with the centre of gravity for the granular material.

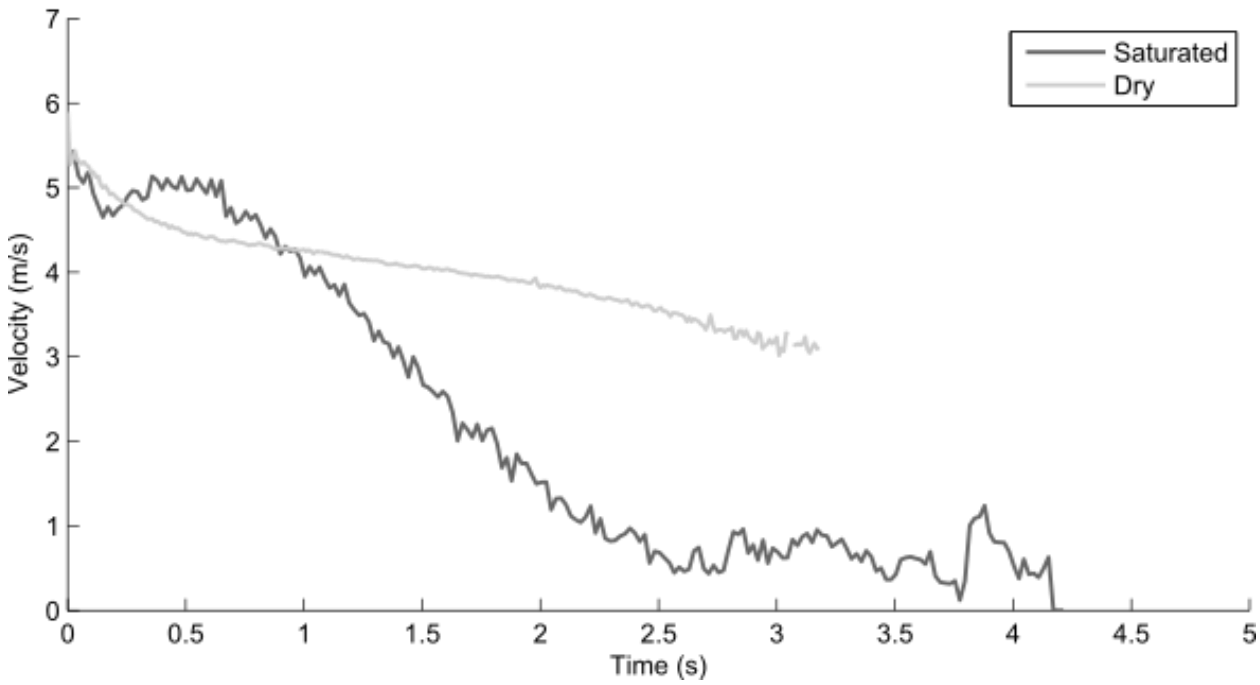

Figure 3.2 Velocity profiles of both a satuarted and dry test with a source volume of 0.4 m^3 measured at the location depicted in Figure 3.1.

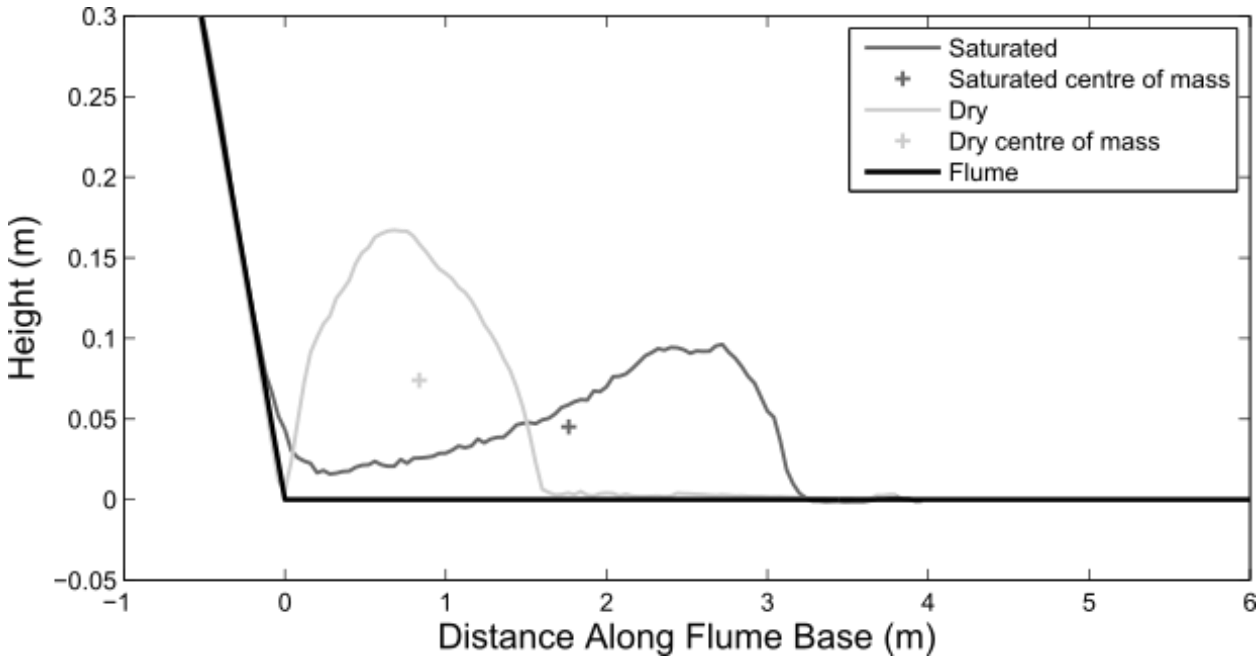

Figure 3.3 Resultant deposit morphology profile for saturated and dry granular tests with a source volume of 0.4 m^3.

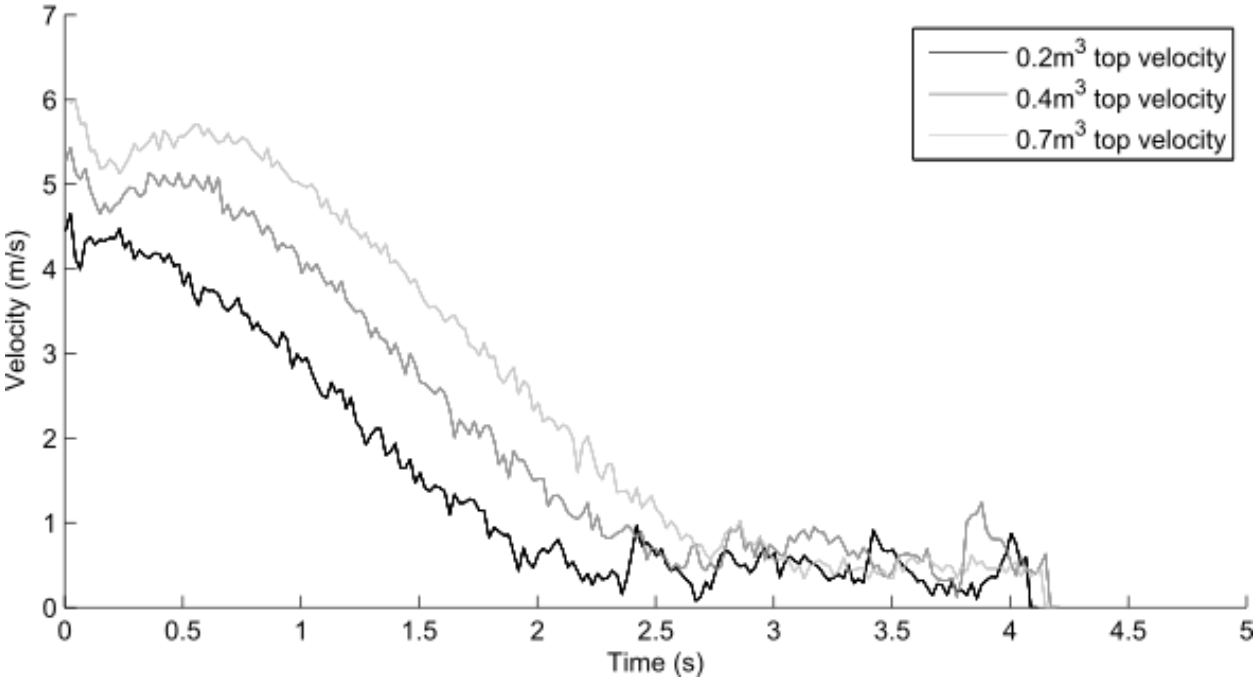

Figure 3.4 Velocity profiles of all three saturated coarse grained material tests.

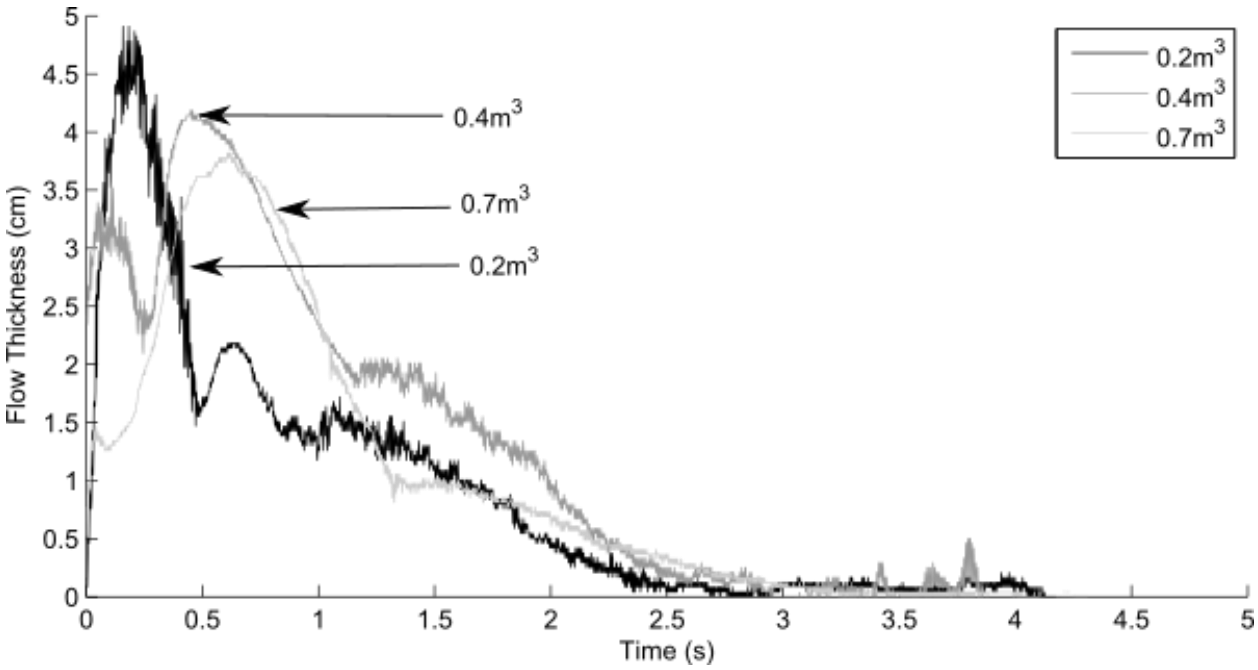

Figure 3.5 Side wall thickness profiles of all three saturated coarse grained tests.

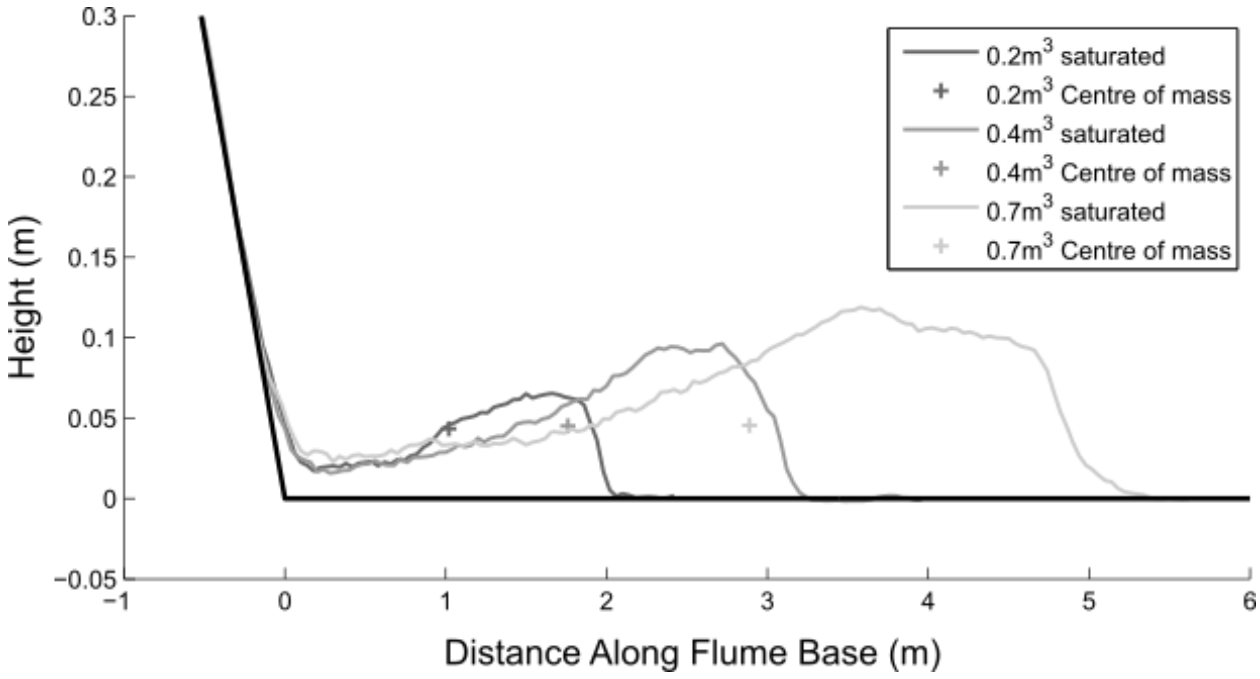

Figure 3.6 Resultant deposit moprpholgy profile for all three saturated coarse grained tests with a varying source volume.

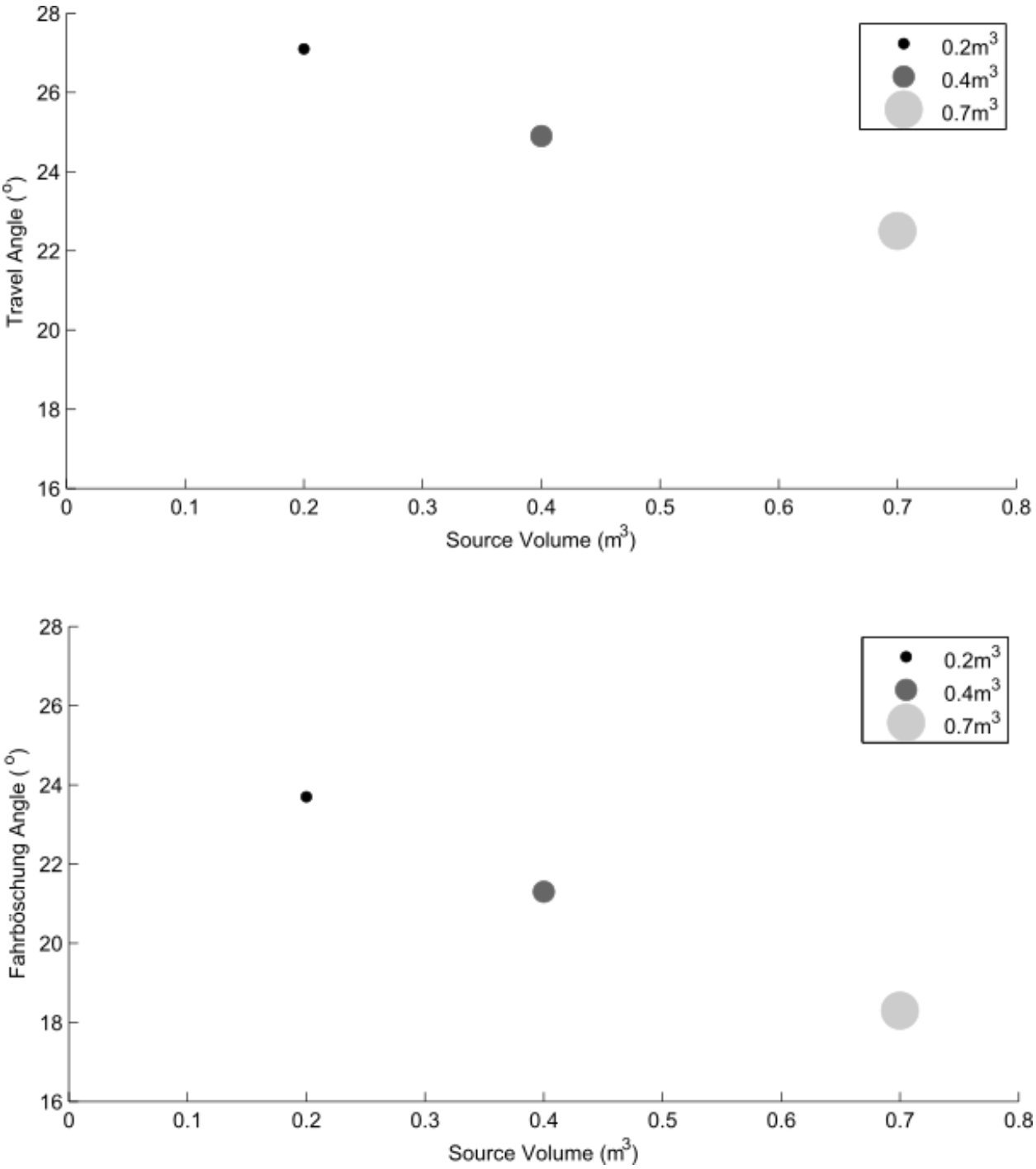

Figure 3.7 The relationship between travel angle, Fahrböschung angle and source volume.

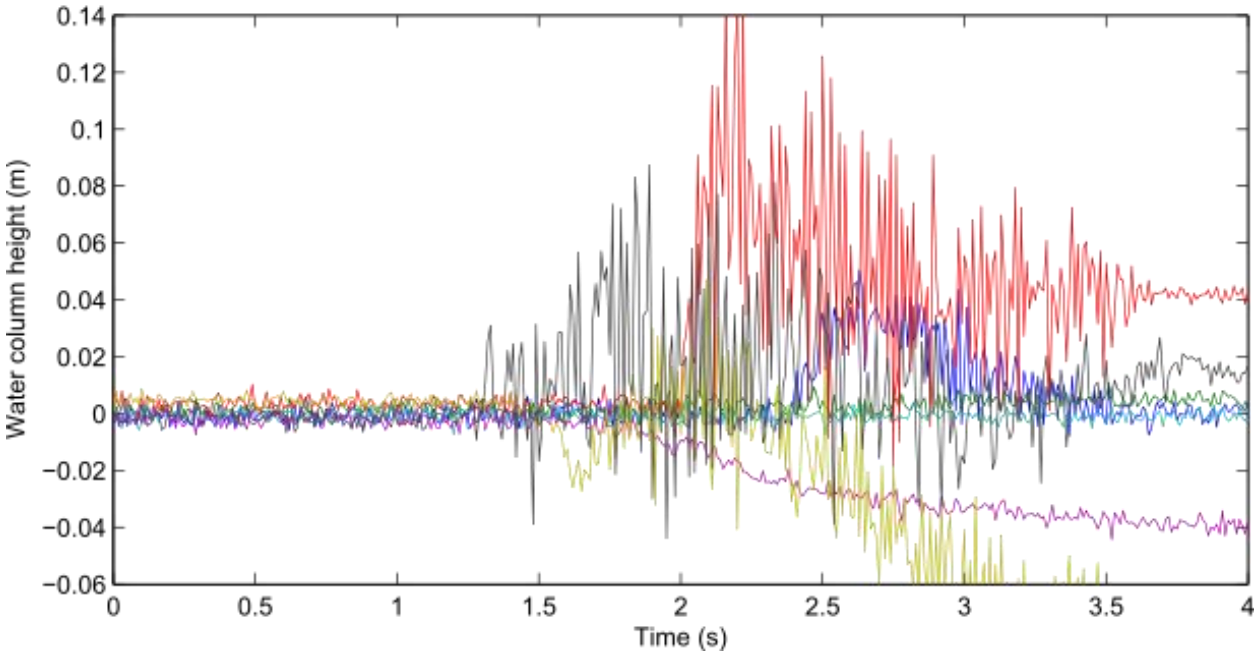

Figure 3.8 Example of PPT data collected from PPTs along the sloping section of the flume for the 0.7 m^3 test.

Figure 3.9 Photo of the dilative behaviour of the saturated fine sand.

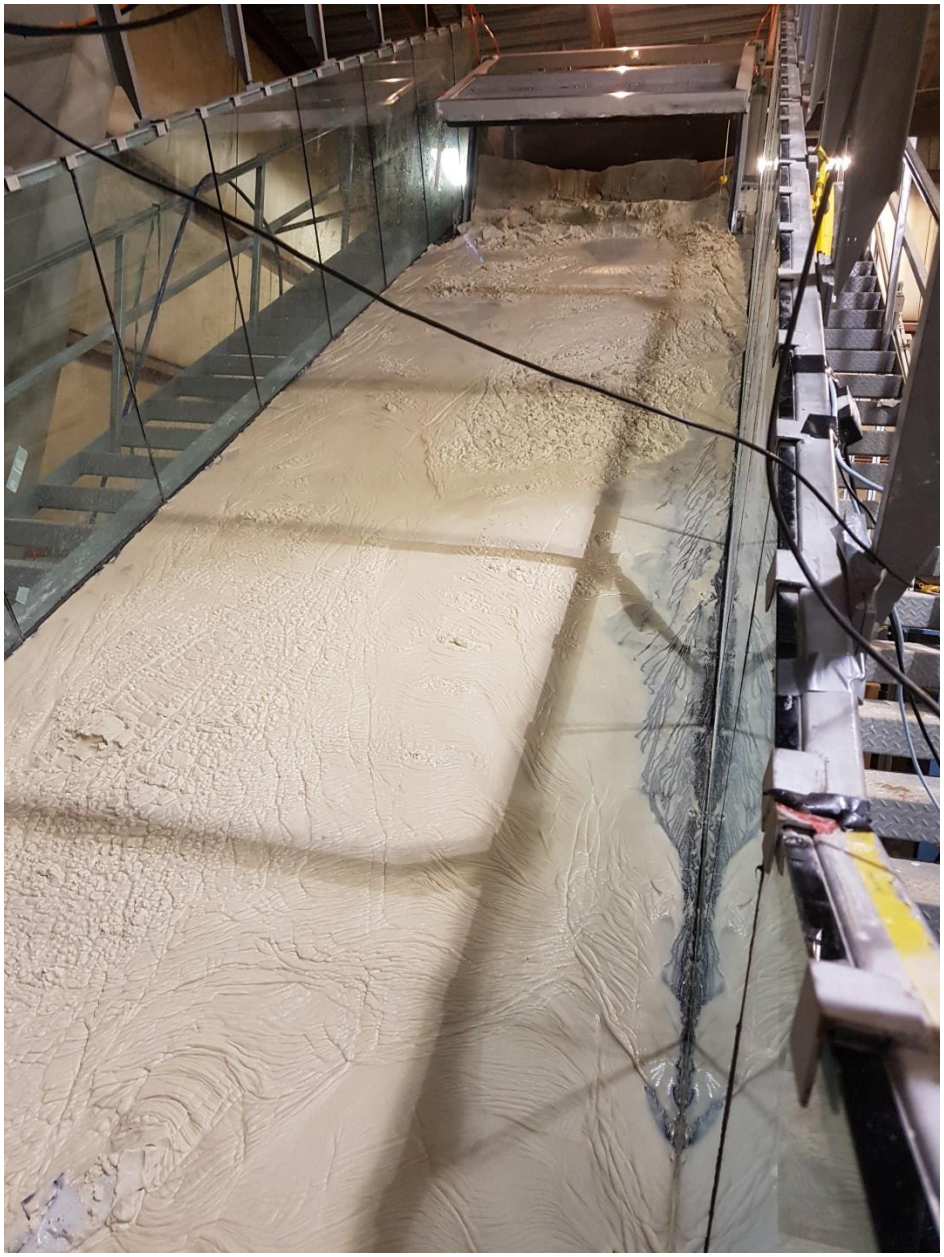

Figure 3.10 Resulting washout deposit of the fine sand tests on the flume slope.

Chapter 4

Conclusions

4.1 Overview

The objective of this research was to investigate the initiation and propagation of liquefaction and the resultant flow mobility due to static triggering in loose granular slopes through testing of physical models. The first phase involved the use a geotechnical centrifuge on a small-scale model, while the second phase involved dam breach experiments conducted on a large-scale landslide flume. The following chapter presents the key concepts and conclusions from both studies. The impact of this work on the field of landslide mobility research is discussed, as well as the recommendations for future research.

4.2 Conclusions drawn from the Research

4.2.1 Objective 1: Exploring the concept of base liquefaction

The main objective of Chapter 2 was to investigate the speed and propagation of a liquefaction front in a simplified physical model and to determine whether or not the liquefaction rate is dependent on the speed of the initial failure. Tests were constructed such that multiple void ratios were tested that were both dense and loose of the critical state. A high-speed camera and multiple PPTs were used to capture the deformation of the model and PWP distribution within the models. It was found that all tests loose of the critical state experienced basal liquefaction, while the dense tests failed under a mechanism of erosion of the base. From the liquefied tests, it is evident that the velocity of the liquefaction front occurs at an order of magnitude greater than the velocity of shearing of the initial failure. Due to the fast nature of the test and the length of the physical model, the entire extent of the base experienced liquefaction.

4.2.2 Objective 2: Development of testing techniques for dam breach experiments

The objective of Chapter 3 was to investigate the shear behavior of saturated granular material in dam break experiments conducted on an inclined plane. Multiple tests at different volumes using either fine sand or coarse grained material were performed to identify experimental challenges, develop testing techniques for saturated granular material and provide preliminary results on the impact of volume size on the mobility of the landslide. With future work, these results can be used to develop a large-scale testing program. Data was collected using two high-speed cameras, one situated to capture the sidewall thickness and the second positioned overhead of the flume to collect the top-down velocity. Multiple PPTs were installed along the base of the flume to capture transient pore pressure results. Results for the coarse grained material showed that saturation of the source volume results in a higher degree of flow mobility with respect to a dry source of the same volume. The addition of water in the coarse grained source volume was observed to decrease the basal friction resulting in higher mobility. Higher mobility was also observed at larger volumes of source material. However, the results of the testing program also showed that collecting pore pressure data of such high mobility flows is extremely challenging and that additional work is required to overcome these issues.

Testing of a saturated fine sand emphasized the fact that dam breach experiments with this material can be difficult to conduct. Multiple tests were conducted trying to create a highly mobile flow. Each test resulted in a soil mass that dilated upon shearing. Attempts were made to pre-liquefy the soil via use of a concrete vibrator; however, this appeared to have the opposite result and densified the soil. When conducting these tests in the future, special care should be taken to construct the model so that the soil is loose and contractile. One possible way of doing this would be to have a sieve that the soil passes through immediately after the sedimentation of the soil into the release box. Another suggestion would be to install a type of upward hydraulic gradient system that would liquefy the soil from the bottom-up prior to removal of the hydraulic boundary condition.

4.3 Potential Impact of Research

This investigation has shown that if a soil is sufficiently loose, the soil will be liquefiable along the entirety of the base of the model. The identification of this mechanism should be considered when considering the potential of landslide hazards in fine sand. Any area in which groundwater is able to build up, and the soil is loose, should be considered an area of concern. Densification of the soil should be conducted, or the groundwater controlled, so that liquefaction cannot occur. As mentioned, the extent to which the basal liquefaction extends is unknown.

With respect to the dam breach experiments, it has been shown that fine sand can be extremely hard to liquefy if the soil is not loose enough, or if the force of matrix suction is too great. Ways to overcome these issues have been proposed for future researchers. As for the coarse grained material, results have shown that the saturation of the material increases the mobility of the flow. This program has set up future researchers to continue the investigation into the effect that PWP has on the mobility of granular flows.

4.4 Next Steps

The results collected from this research endeavor have provided further insight into the area of study of high mobility landslides. However, as is the nature of research, additional unanswered questions have arisen during the process. These questions pertain to the effect of thickness and grain size on slope mobility and are addressed in the following sections.

4.4.1 Centrifuge Modelling

In further work, it would be of benefit to develop a method to predict the degree of consolidation of the sample during spin-up of the centrifuge. This would allow for tests to be designed such that the thickness of the slope remains constant among all tests. Consistent soil thickness will ensure that the drainage path also remains the same from test to test. With a consistent drainage path, comparisons could be made between the temporal duration of liquefaction for each test, and how that differs with a change in void ratio. Another area of research that requires investigation is how a change in void ratio affects slope

mobility. Iverson et al. (2015) hypothesizes that a change in void ratio of only 0.02 less than the critical is the difference between a highly mobile liquefied soil and a dilative slump. An investigation needs to be undertaken to prove whether this is correct. Additional centrifuge tests could also be performed with a longer runout length to determine the full extent of the liquefaction of the base.

4.4.2 Flume Facility

Future research utilizing the flume facility could be conducted to verify how a change in the degree of saturation of the coarse grained material affects the mobility of the landslide. This would allow for a spectrum of tests to be conducted, which could help determine the exact role that PWP plays in landslide mobilization. Utilizing different particles would also be of interest. Larger particle sizes experience more collisional flow, so it would be fascinating to see how the saturation of the material influences the flow behavior. As for the fine sand, developing a mechanical method of liquefying the soil prior to release would be of benefit so that comparisons could eventually be made between the mobility of fine and coarse grained material. However, before any further testing can be conducted, it is crucial that new and accurate PPTs be installed to monitor PWP. Care must be taken to minimize the water within the sensor system and ensure complete saturation of the PPT. With proper installation, the entrapment of air will be minimized, leading to higher quality data. Without the information collected by the PPTs, a complete story of the effect of PWP on landslide mobility cannot be told.

4.4.3 Numerical Modelling

The scope of this research program was limited to physical modelling; however, a great opportunity has been identified for numerical modelers. Current numerical modelling considers slope failure from either a finite element method (FEM) standpoint, which looks at the initial section of a slope to fail, or a depth averaged numerical method (DAN) standpoint, which focuses on the mobility of a failed slope. This research, however, has shown that the liquefaction of the base is contingent upon an initial failure, and that for this scenario to be correctly modelled numerically, a combination of both FEM and DAN analysis must be conducted. Thus, there is an excellent opportunity for a future researcher to bridge the gap

between the FEM and DAN models, so that liquefaction events can be accurately numerically modelled, the inner workings of a future landslides better understood, and their negative impacts, hopefully, avoided.